THE POST-SHOCK CHEMICAL LIFETIMES OF OUTFLOW TRACERS AND A POSSIBLE NEW MECHANISM TO PRODUCE WATER ICE MANTLES

Edwin A. Bergin[1], Gary J. Melnick[1], and David A. Neufeld[2]

[1] Harvard-Smithsonian Center for Astrophysics, MS-66, 60 Garden St., Cambridge, MA 02138; ebergin, gmelnick@cfa.harvard.edu

[2] Department of Physics and Astronomy, The Johns Hopkins University, 3400 North Charles Street, Baltimore, MD 21218; neufeld@pha.jhu.edu

ABSTRACT

We have used a coupled time-dependent chemical and dynamical model to investigate the lifetime of the chemical legacy left in the wake of C-type shocks. We concentrate this study on the chemistry of H_2O and O_2, two molecules which are predicted to have abundances that are significantly affected in shock-heated gas. Two models are presented: (1) a three-stage model of pre-shock, shocked, and post-shock gas; and (2) a Monte-Carlo cloud simulation where we explore the effects of stochastic shock activity on molecular gas over a cloud lifetime. For both models we separately examine the pure gas-phase chemistry as well as the chemistry including the interactions of molecules with grain surfaces. In agreement with previous studies, we find that shock velocities in excess of 10 km s^{-1} are required to convert all of the oxygen not locked in CO into H_2O before the gas has an opportunity to cool. For pure gas-phase models the lifetime of the high water abundances, or "H_2O legacy", in the post-shock gas is $\sim 4 - 7 \times 10^5$ years, independent of the gas density. A density dependence for the lifetime of H_2O is found in gas-grain models as the water molecules deplete onto grains at the depletion timescale.

Through the Monte Carlo cloud simulation we demonstrate that the time-average abundance of H_2O – the weighted average of the amount of time gas spends in pre-shock, shock, and post-shock stages – is a sensitive function of the frequency of shocks. Thus we predict that the abundance of H_2O, and to a lesser extent O_2, can be used to trace the history of shock activity in molecular gas. We use previous large-scale surveys of molecular outflows to constrain the frequency of 10 km s^{-1} shocks in regions with varying star-formation properties and discuss the observations required to test these results. We discuss the post-shock lifetimes for other possible outflow tracers (e.g. SiO, CH_3OH) and show that the differences between the lifetimes for various tracers can produce potentially observable chemical variations between younger and older outflows. For gas-grain models we find that the abundance of water-ice on grain surfaces can be quite large and is comparable to that observed in molecular clouds. This offers a possible alternative method to create water mantles without resorting to

grain surface chemistry: gas heating and chemical modification due to a C-type shock and subsequent depletion of the gas-phase species onto grain mantles.

Subject headings: ISM: chemistry; ISM: molecules - stars - shock waves

1. Introduction

The importance of molecular gas as the material from which stellar and planetary systems are made has led numerous investigators to examine the chemical processes that combine atoms into molecules. Over the past two decades these studies have gradually increased in both complexity and fidelity and can roughly be divided into three generations. The first generation chemical model solved the chemical rate equations at equilibrium, or steady-state, and demonstrated the importance of ion-molecule reactions in driving the gas-phase chemistry (Herbst & Klemperer 1973). The second generation of models utilized the later availability of increased computing power to study the time evolution of chemical abundances (Prasad & Huntress 1980; Graedel, Langer, & Frerking 1982). These models, labeled as "pseudo-time dependent" – "pseudo" because the chemistry evolves with fixed physical conditions – used observed physical properties of dense molecular cores ($T_k \sim 10 - 30$ K, n_{H_2} = 10^{4-6} cm^{-3}) to show that chemical equilibrium was reached in $\sim 10^{6-8}$ years. Pseudo-time dependent models represent the most prevalent chemical model and have been quite successful in describing the chemistry of quiescent regions in both dark and giant molecular cloud cores (Lee et al. 1996; Bergin et al. 1997).

Second generation chemical models operate under one simplifying assumption: that the molecular gas undergoes no dynamical evolution as it chemically evolves. However, molecular clouds are certainly dynamically evolving objects. The widespread occurrence of superthermal widths in molecular lines suggests that, overall, the evolution of molecular clouds is not simple quiescent evolution at a single gas temperature. Moreover, the formation of a low- or high-mass star from a molecular condensation involves a collapse that increases the density by many orders of magnitude. It has also been recognized that the birth of a protostar is associated with a period of intense mass loss, which manifests itself in energetic winds, bipolar jets, and large-scale outflows (c.f. Lada 1985; Bachiller 1996). The impact of energetic flows on surrounding quiescent gas can compress and heat the gas, in some cases providing enough energy to overcome endothermic barriers of chemical reactions, sputter or destroy grains, or even dissociate molecules. The result can be a considerably different chemical composition in the shocked gas than observed in quiescent material. Since molecules are the primary coolants of the gas, any chemical change induced by collapse or shocks can also alter the ensuing physical evolution of the cloud. To address such concerns, a third generation of chemical models has been constructed to build on the successes of previous generations by combining chemistry with dynamics. These models have been principally directed towards investigating the chemistry of core and star formation (c.f. Prasad et al. 1987; Rawlings et al. 1992; Bergin & Langer 1997), the physical and chemical structure of shocked gas (c.f. Draine & McKee 1993), or even complex scenarios in which gas is cycled between low and high density through recurrent episodes of low-mass star formation (Charnley et al. 1988a).

One goal of coupled astrochemical models is to search for and isolate specific molecular species that serve as signposts of particular dynamical events, such as shocks. Coupled models of shocked molecular gas have isolated one molecule in particular, H_2O, which is predicted to form in large abundance in shock-heated gas (Draine, Roberge, & Dalgarno 1983; Kaufmann & Neufeld 1996a,b); if temperatures in the shocked gas exceed 400 K, the endothermic barriers of a few key chemical reactions are exceeded and all of the available oxygen not locked up in CO will be driven into H_2O. This led to the assertion that water emission is a ubiquitous tracer of shock-heated gas (Neufeld & Melnick 1987). Unfortunately, due to constraints imposed by the earth's atmosphere, the detection of H_2O in interstel-

lar clouds from ground-based observatories is a challenging task. Nevertheless, several studies have observed, and detected, transitions of isotopic water ($H_2^{18}O$), and even H_2O (c.f. Jacq et al. 1988; Knacke & Larson 1991; Zmuidzinas et al. 1994). Quite recently, absorption from warm ($T_{gas} > 200$ K) water vapor has been unambiguously detected by the Infrared Space Observatory (ISO) towards hot stars (Helmich et al. 1996; van Dishoeck & Helmich 1996), and in emission in HH54 (Liseau et al. 1996). The inferred water abundance in these sources is $\sim 1 - 6 \times 10^{-5}$, much larger than predicted by chemical models run for cold quiescent conditions ($x(H_2O)$ $\sim 10^{-7}$), and is consistent with water production in warm gas either though high-temperature chemistry – as would apply in shock-heated gas or in the near vicinity of embedded sources – or via evaporation of water-ice mantles.

An important question yet to be addressed by coupled dynamical and chemical models of shocked gas in molecular clouds is how long the high abundances of water and other molecules persist following the passage of a shock. As we will demonstrate, the time needed for shock-heated gas to return to its pre-shock temperature is several orders of magnitude less than the time required for the gas to return to its pre-shock chemical composition. Thus, the enhanced abundances of water and other species could potentially exist long after the dynamical effects of a shock passage are dissipated. Therefore, the chemistry inside a cloud is reflective of, and can be used to probe, the physical shock history of the molecular gas.

Motivated by these questions, we present the results of a coupled dynamical and chemical study of molecular gas that is subjected to shocks with velocities greater than 10 km s^{-1}. In particular, we follow the time dependence of the chemistry in a shock-heated gas layer as it cools and the quiescent time-dependent chemistry is ultimately re-established. We present models examining this evolution using pure gas-phase chemistry as well as chemistry which includes the interaction of molecules with grain surfaces.

In Section 2 we discuss the combined chemical and dynamical model. In Section 3 we use published surveys of molecular outflows to investigate the average rate at which shocks with a minimally sufficient velocity to affect the water chemistry – 10 km s^{-1} – pass a given region of a cloud. Section 4 presents the results from our combined models along with one example of quiescent chemical evolution. Two models are presented: (1) a three-stage model of pre-shock, shocked, and post-shock gas; and, (2) a Monte-Carlo cloud simulation in which the results from Section 3 are used to examine the effects of stochastic shock activity on molecular gas over a cloud lifetime. Section 5 discusses the importance of these results on chemical models of molecular gas and also reviews the observations required to test these models. In Section 6 we summarize our results.

2. Dynamical and Chemical Model

2.1. Shocks and Chemistry

Detailed models of magnetohydrodynamic (MHD) shocks in dense molecular clouds have been created by a number of authors. For a comprehensive discussion of various models the reader is directed to the review in Draine & McKee (1993). Briefly, MHD shocks in interstellar gas are divided into two categories: (1) J-type shocks where flow variables are discontinuous across the shock; and, (2) C-type shocks where the flow variables are continuous across the shock front. For J-shocks the energy dissipation occurs in a thin layer where the temperature increase is high enough to destroy molecules. In C-type shocks propagating through a magnetic medium with low ionization (the case for dense molecular gas) the gas is frictionally heated in a thicker layer through the process of ambipolar diffusion wherein ions tied to the field drift through the neutral fluid. The temperatures produced by this

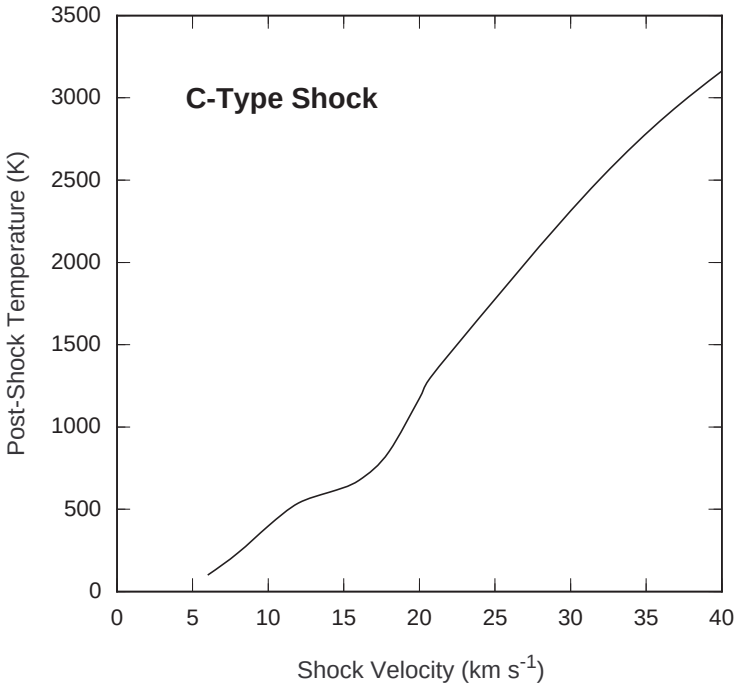

Fig. 1.— Maximum attained gas temperature as a function of shock velocity for density of $n_{H_2} = 10^5$ cm^{-3} (taken from Kaufman & Neufeld 1996b). The slight drop in temperature at ∼15 km s^{-1} is due to the onset of H_2O formation and cooling.

process are as high as several thousand Kelvins, but the gas remains in molecular form (Mullan 1971; Draine 1980). In addition, the gas compression in the wake of C-shocks in the region of the temperature peak is not exceedingly large (c.f. Draine & Roberge 1982); to first order, the neutral density in the gas which will be most affected by the temperature increase is approximately constant. The magnitude of the heating depends on the pre-shock density, the strength of the magnetic field, and the velocity of the shock. For the purposes of this paper we are mostly concerned with the non-dissociative C-type shocks that drive observed molecular outflows. We account for the possibility of dissociative shocks in the more comprehensive cloud model presented in Section 4.4.

In the models shown here we are solely concerned with the chemistry in the post-shock gas, which is largely driven by the gas temperature, molecular hydrogen density, and the visual extinction. To simplify the computational task, we adopt many of these conditions from detailed MHD shock models (e.g., Kaufman and Neufeld 1996a,b: hereafter KN96a and KN96b), including the variations in these parameters with both time and shock velocity. For C-shocks, the post-shock H_2 density in the region of the temperature maximum can be held constant. In addition, most shock models assume that the post-shock gas is shielded from dissociating radiation, an assumption we adopt as well. Thus, the most important remaining parameters to be extracted from the MHD shock models are the velocity-dependent temperature profiles and their time evolution.

KN96b present a self-consistent calculation of the heating, cooling, and chemistry of a MHD shock wave propagating through dense ($n_{H_2} = 10^{4-6.5}$ cm^{-3}) molecular gas with low ($< 10^{-7}$) ionization. The magnetic field in their model is assumed to be perpendicular to the direction of shock propagation with a value of $B = (n_H/cm^{-3})^{1/2}$ μG. The assumed values for the ionization fraction and magnetic field strength are consistent with those estimated in molecular clouds (e.g. Guélin et al. 1982; Troland & Heiles 1986). In Figure 1 we show the maximum shock temperature as a function of the shock velocity (adapted from KN96b). This dependence

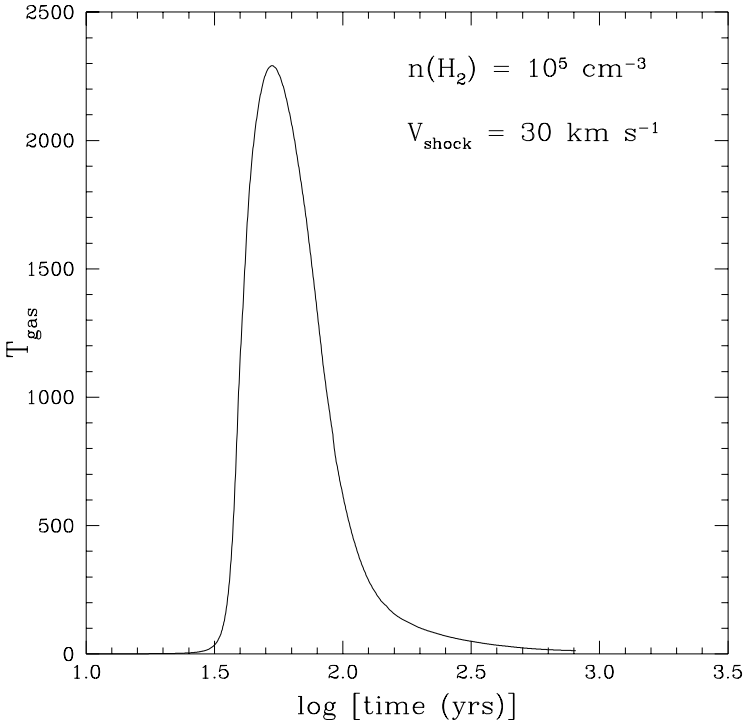

Fig. 2.— Shock temperature as a function of time for $v_s = 30$ km s^{-1} and $n_{H_2} = 10^5$ cm^{-3} (provided by M. Kaufman).

is shown for a pre-shock molecular hydrogen density of 10^5 cm^{-3}, but the maximum post-shock temperature is only weakly dependent on the density (KN96b). Clearly the gas temperature is a strong function of the shock velocity, and is essentially a reflection of the strength of the frictional heating created by ambipolar diffusion.

Another important parameter required to examine the chemistry of post-shock gas is the amount of time the temperature remains at elevated levels. In Figure 2 we present the temperature as a function of time during the passage of a 30 km s^{-1} shock in a medium with a pre-shock density $n_{H_2} = 10^5$ cm^{-3}. These data have been kindly provided by M. Kaufman using the code described in KN96a,b. The effect of the shock is clearly evident as the gas temperature rises to greater than 2000 K in less than 100 years. After the passage of the shock, the gas rapidly cools within a few hundred years. The principal coolants of the gas are H_2, H_2O, and CO. Thus, the passage of a 30 km s^{-1} shock could heat the gas from T_{gas} = 10–30 K to $\sim$ 2000 K, and this gas will return to 30 K within a few hundred years.

2.2. Chemical Model

In these calculations we have used the chemical model initially described in Bergin, Langer, & Goldsmith (1995) and updated in Bergin & Langer (1997). These papers examined the gas-phase chemical evolution including grain surface molecular depletion and desorption. For this calculation we have used both the gas-phase UMIST RATE95 chemical network (Millar et al. 1997) and the gas-grain adaption of this network described in Bergin & Langer (1997). Thus, we separately examine the pure gas-phase chemistry and the evolution including grain processes. The gas-grain models include depletion onto grain surfaces and desorption via three desorption mechanisms: cosmic-ray-induced heating, photodesorption, and simple thermal evaporation (see Bergin, Langer, & Goldsmith 1995). For these models we use the binding energies of molecules on an SiO_2 grain surface.

For a given calculation the adjustable variables are the density of molecular hydrogen, n_{H_2}, the factor by which the external UV field is enhanced above the average galactic interstellar radiation field, G_o, the gas temperature, T_{gas}, and

the visual extinction to the center of the cloud, A_V. For gas-grain models, the dust temperature (T_{dust}) is also a variable. The initial chemical conditions are taken from Millar et al. (1991), and assume that the carbon, silicon, iron, sulfur, sodium, potassium, and magnesium are in ionized form, while the oxygen and nitrogen atoms are neutral. All species are assumed to be depleted relative to their solar abundances, while the heavy atoms (e.g., Fe, Mg) are assumed to be more severely depleted than carbon, oxygen, and nitrogen.

For chemical models of interstellar shocks, it is particularly important that the chemical network contains rate coefficients appropriate for high-temperature chemistry. To minimize such concerns, we only discuss in detail results for a few simple carbon- and oxygen-bearing species (C, CO, HCO^+, O, O_2, OH, and H_2O) whose chemistry is well characterized at both high and low temperatures. As mentioned earlier, when temperatures exceed ∼400 K, water is rapidly formed in the gas phase through the following series of neutral-neutral reactions

$$O + H_2 \rightarrow OH + H \qquad \text{(R1)}$$

$$OH + H_2 \rightarrow H_2O + H \qquad \text{(R2)}$$

(Elitzur & de Jong 1973; Elitzur & Watson 1978). Both of these reactions possess significant activation barriers ($E_a(R1) = 3160$ K; $E_a(R2) = 1660$ K). For very high temperatures, molecular oxygen will be destroyed by reaction R3,

$$O_2 + H_2 \rightarrow OH + OH \qquad \text{(R3)}$$

($E_a(R2) = 28190$ K), and eventually processed into H_2O through reaction R2. We examine in detail the temperature dependence and efficiency of reactions R1–3 in the following section.

The chemical network includes many other species beyond the simple species we emphasize in this paper and, unless otherwise noted, these species have been included in the model runs. Because we do not have the same confidence in the high-temperature chemical reactions that form these species, we do not provide their predicted abundances. The UMIST database contains rate equations for gas temperatures between 10 – 50 K (Millar, Farquhar, & Willacy 1997), a more consistent calculation for other potentially important shock tracers, such as SiO or SO, requires the incorporation of other reactions such as those estimated for sulphur-bearing species in Pineau des Forêts et al. (1993). However, in Section 5.2 we do discuss the relevance these results might have on the abundances and post-shock lifetimes of some of these "shock tracers."

Careful attention has also been paid to the accuracy of the low-temperature reaction rates, although we have sought to minimize this concern through the use of the UMIST database. Of particular importance for the abundance of water at low temperatures are two reactions that have been the subject of considerable debate. These are the dissociative recombination rate of H_3^+, and the branching ratios of the H_3O^+ recombination reaction. For H_3^+, the UMIST RATE95 database has adopted a rate of $\alpha(H_3^+) = 3 \times 10^{-8} T^{-0.5}$, from Smith and Spanel (1993). This rate has been slightly revised by the recent measurements of Sundström et al. 1994. The adoption of the more recent value will not alter our results. Recently, there have been two studies of the H_3O^+ dissociative recombination branching ratios (Williams et al. 1996; Vejby-Christensen et al. 1997). The branching paths are:

$$\begin{aligned} H_3O^+ + e^- &\rightarrow H + H_2O & f_1 \quad \text{(R4)} \\ &\rightarrow OH + H_2 & f_2 \\ &\rightarrow OH + 2H & f_3 \\ &\rightarrow O + H + H_2 & f_4 \end{aligned}$$

where f_{1-4} are the branching ratios. Vejby-

Christensen et al. (1997) using an ion storage ring measured $f_1 = 0.33$, $f_2 = 0.18$, $f_3 = 0.48$, and $f_4 = 0.01$, while Williams et al. (1996) used an ion flow tube to measure $f_1 = 0.05$, $f_2 = 0.36$, $f_3 = 0.29$, $f_4 = 0.3$. The overall OH production predicted by these two studies are in reasonable agreement, which is important since OH reacts with O to form O_2. However, the measurements differ significantly in their production of water and atomic oxygen. For the following calculations we have used the branching ratios estimated by Vejby-Christensen et al. (1997). In order to examine the sensitivity of these results to this choice, we present one case using the other branching ratios.

3. Shock Timescales in Molecular Clouds

Before we examine the timescale for the reassertion of quiescent chemistry after the passage of a shock, it is useful to examine how often molecular material in molecular cores is subjected to 10 km s^{-1} shocks. The choice of this particular shock velocity is discussed in Section 4.2. To estimate the rate at which a parcel of molecular gas might be subjected to a 10 km s^{-1} shock, we have used a method outlined in Margulis, Lada, and Snell (1988). Margulis and Lada (1986) surveyed a $\sim 0.5^\circ \times 2^\circ$ region of the Mon OB1 molecular cloud in the emission of ^{12}CO and identified nine separate molecular outflows. To examine the effect of the molecular outflows on the dynamics of the entire molecular core, Margulis et al. (1988) estimate the total momentum added to the cloud by the outflows. The momentum of an outflow is estimated by either: (a) integrating directly over the mass $\times$ velocity in each velocity channel in the line wings, ignoring the possible contribution of outflow material hidden by the line core; and/or, (b) assuming that the entire outflow is at a constant velocity, which is equated to the maximum observed flow velocity (c.f. Lada 1985). Using method (a) provides a lower limit to the momentum, because it ignores the inclination of the outflow and, because of the difficulty of differentiating the line wings from the core, also ignores the mass in the line core. In contrast, method (b) is a strict upper limit, because it assumes that all of the mass in the flow is at the highest observed velocity.

Using method (a) and the momenta listed in Table 2 of Margulis et al. (1988), the total momentum generated by the observed outflows in Mon OB1 is 163 $M_\odot$ km s^{-1}. Momentum conservation requires that 16 $M_\odot$ of molecular material will have been swept up when the outflows have reached a velocity of 10 km s^{-1}. Since the total mass in the portion of Mon OB1 surveyed is 3 $\times 10^4$ $M_\odot$ (Margulis and Lada 1986), only 0.05 percent of the total mass will be affected by the energetic flows. Thus, in the momentum conserving case, it requires $\sim$1900 generations of similar star-formation activity for the entire surveyed area to have experienced a shock of $\sim$10 km s^{-1}. Assuming that the average duration of the outflow phase is $\sim 2 \times 10^4$ year (Staude and Elsässer 1993), then an upper limit to the shock timescale, τ_s, for gas in Mon OB1 to be hit by 10 km s^{-1} shocks is $< 4 \times 10^7$ years. Because the outflow momentum estimates are strict lower limits (see discussion of method (a) above), and due to the assumption that subsequent generations of star-formation activity occurs continuously, this timescale is an upper limit. Similarly, we can use the momenta calculated via method (b) to set a lower limit for this timescale. Using method (b), Margulis et al. (1988) calculate the total momentum to be 883 $M_\odot$ km s^{-1}, which is 3 percent of the total mass of Mon OB1. Therefore, $\sim$340 generations of similar star-formation activity are required to process the entire core by 10 km s^{-1} shocks, and the lower limit to the timescale is τ_s(Mon OB1) $> 7 \times 10^6$ year. We have performed a similar analysis using the observations of L1641 in Morgan et al. (1991) and find similar results, i.e., τ_s(L1641)$\sim 0.6-2.7\times 10^7$ years.

It's important to note that this "cloud-average" approach is useful for investigating the poten-

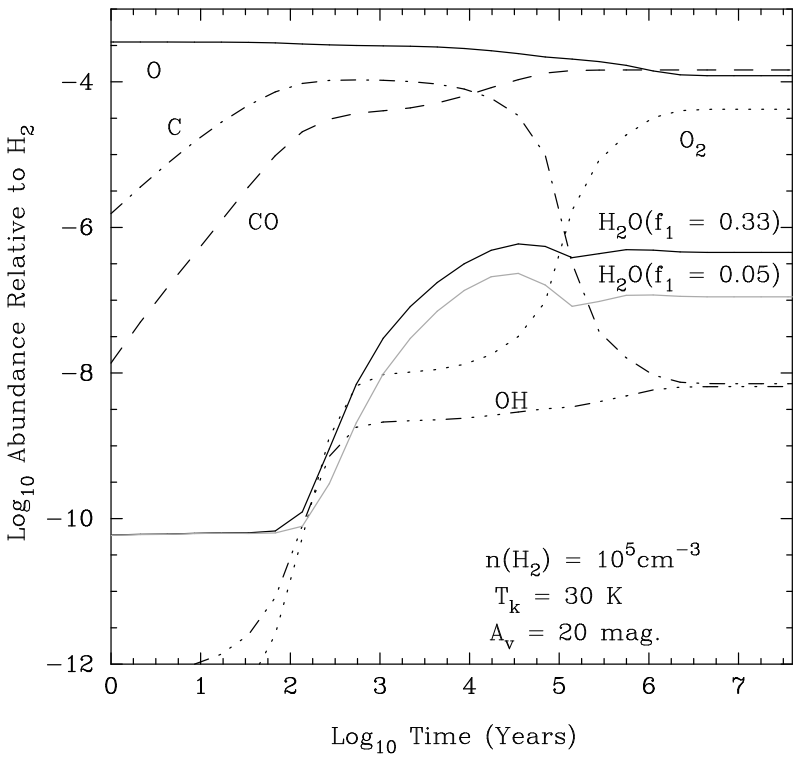

Fig. 3.— Time evolution of chemical abundances relative to H_2 for quiescent physical conditions. The evolution of the H_2O abundance is shown for two values of the H_3O^+ branching ratio (discussed in Section 3).

tial of shocks to alter the global composition of a cloud. Clearly though, this is an oversimplification. In reality, an observer will see portions of a cloud that are experiencing active star formation, for which the local value of τ_s may be $\ll 10^6$ years, while more quiescent regions of the same cloud may have local values of τ_s closer to a few times 10^7 yrs, the upper limit quoted above. For instance, NGC 1333 is an example of a molecular core where a cluster of outflows has been detected within a $15' \times 15'$ (1.5 × 1.5 pc) area (see Liseau et al. 1998, Warin et al. 1996 and references therein). Thus, *locally* the shock timescale in NGC 1333 may be below the global value of $\sim 10^7$ years. Another example is the Orion Nebular Cluster where several thousand stars are estimated to have been formed within the past 1-2 million years (Hillenbrand 1997). If each new star has an an associated outflow phase, it is certainly possible that the shock timescale *in the dense core associated with this cluster (OMC-1)* can be reduced to values well below the global value. As will be shown, a range in the values of τ_s between $< 10^6$ and $> 10^7$ years spans a large range in chemical outcomes and may ultimately prove to be the cause of strong compositional gradients within clouds.

4. Results

In this section we present the results of the coupled dynamical and chemical model of molecular gas that is subject to shocks with a range of velocities. For quiescent conditions, we assume, unless otherwise noted, that $n_{H_2} = 10^5$ cm^{-3}, $T_{gas} = T_{dust} = 30$ K, $G_o = 1$, and $A_V = 20$ mag. These conditions are similar to those observed in Giant Molecular Cloud (GMC) Cores, the sites of massive star formation (Goldsmith 1987).

4.1. Quiescent Chemistry

In Figure 3 we present the time dependence of the gas-phase chemistry for the quiescent conditions appropriate in GMC cores. In this figure we also show the water abundance calculated using two different values for the H_3O^+ dissociative recombination branching ratios (see discussion in Section 2.2). The observed time evolution of chemical abundances is quite similar to other current gas-phase chemical models (Lee et

al. 1996; Millar et al. 1997). Examination of the evolution shows that the carbon abundance peaks at early times ($t \sim 10^4$ years for $n_{H_2} = 10^5$ cm^{-3}), while for later times all carbon is locked into CO. Equilibrium is reached after $\sim 3 \times 10^6$ years, when the dominant oxygen reservoirs are O, CO, and O_2. In addition, due to cosmic-ray-induced photodissociation of O_2 (Sternberg & Dalgarno 1995), most oxygen remains in atomic form, although the total amount of oxygen in O_2 ($2 \times x(O_2)$) is similar to the abundance of atomic oxygen. The steady-state water abundance is different for the two measured branching ratios; for $f_1 = 0.33$ the abundance is $x(H_2O) \sim 4.5 \times 10^{-7}$, while for $f_1 = 0.05$, $x(H_2O) \sim 1.0 \times 10^{-7}$. For all other calculations we use $f_1 = 0.33$.

4.2. High-Temperature Chemistry

In Figure 4 we present the dependence of the water abundance on both time and temperature, while Figure 5 presents a similar plot for O_2. The models are for pure gas-phase chemistry where we allow the chemical evolution to proceed for 10^5 years with $T_{gas} = 30$ K, at which point the chemistry is re-initiated and the temperature is increased to the values indicated in Figures 4 and 5. This method allows for appreciable abundances of molecular species to build up in the gas phase at low temperature and makes it easier to gauge the effects of high temperature chemistry. Thus, $t = 0$ in these figures refers to time after 10^5 years of low-temperature or quiescent chemical evolution when the abundances of water and molecular oxygen are $x(H_2O) \sim 4 \times 10^{-7}$ and $x(O_2) \sim 3 \times 10^{-7}$. The results presented in Figures 4 and 5 do not depend in detail on the time the chemistry is allowed to evolve under quiescent conditions.

In Figure 4, for $T_{gas} > 500$ K (corresponding to shock velocities, $v_s > 10$ km s^{-1}), water accounts for all of the oxygen not bound as CO within ∼100 years. For temperatures below ∼400 K, the efficiency of reactions R1 and R2 begins to rapidly decline until $T_{gas} \sim 200$ K where the high-temperature reactions are unimportant compared to the low-temperature formation pathways. In contrast, the abundance of O_2 shown in Figure 5 exhibits the opposite behavior. For $T_{gas} = 400$ K the O_2 abundance increases above the initial value through normal time-dependent chemistry. However, at $t \sim 2 \times 10^5$ years, the abundance of O_2 exhibits a rapid decrease and reaction R3 effectively processes O_2 into H_2O. For even higher temperatures the destruction of O_2 becomes more efficient, although it requires gas temperatures greater than 2000 K, corresponding to $v_s \geq 26$ km s^{-1}, to destroy all O_2 within 100 years.

As demonstrated in Section 2, the post-shock gas will not remain at elevated temperatures for the entire time shown in Figures 4 and 5. Using the cooling information provided in Figure 2, we see that the time for the post-shock gas to cool to below 200 K, what we term the cooling timescale, is ∼ 100 years. Combining the information shown in Figures 2 and 4 suggests that *shocks with velocities > 10 km s^{-1} will convert all of the oxygen to water within a cooling timescale*. The maximum temperatures reached behind shocks with velocities less than 10 km s^{-1} will not be high enough to overcome the activation barriers and the abundance of water should remain relatively unaltered from its quiescent values. This result is similar to that found by KN96a,b who found that the maximum shock velocity for the conversion of O to H_2O is 10 – 15 km s^{-1}. Similarly, shock velocities > 26 km s^{-1} are required to destroy all molecular oxygen within the cooling timescale. While the exact cooling timescale will vary with shock velocity, the cooling will be most efficient when the oxygen is mainly in the form of water – thus, the cooling timescale should not vary appreciably as long as $T_{gas} > 400$ K.

4.3. Three-Stage Chemical Model

We envisage that the chemical evolution of gas in star-forming molecular clouds that have been

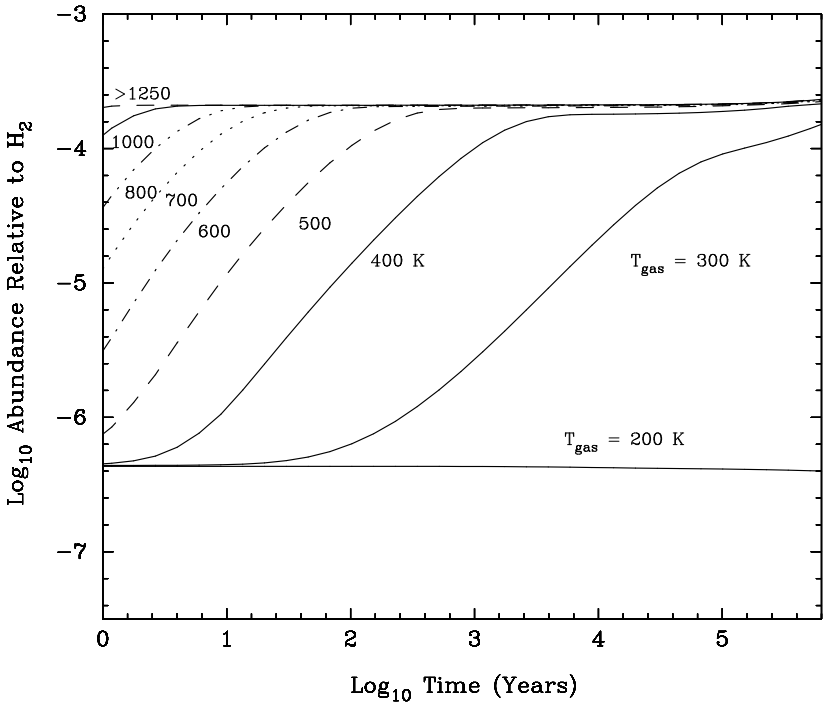

Fig. 4.— Abundance of H_2O as a function of time and gas temperature. The times listed on the abscissa are times after $\sim 10^5$ years of evolution with $T_{gas} = 30$ K (see Section 4.1).

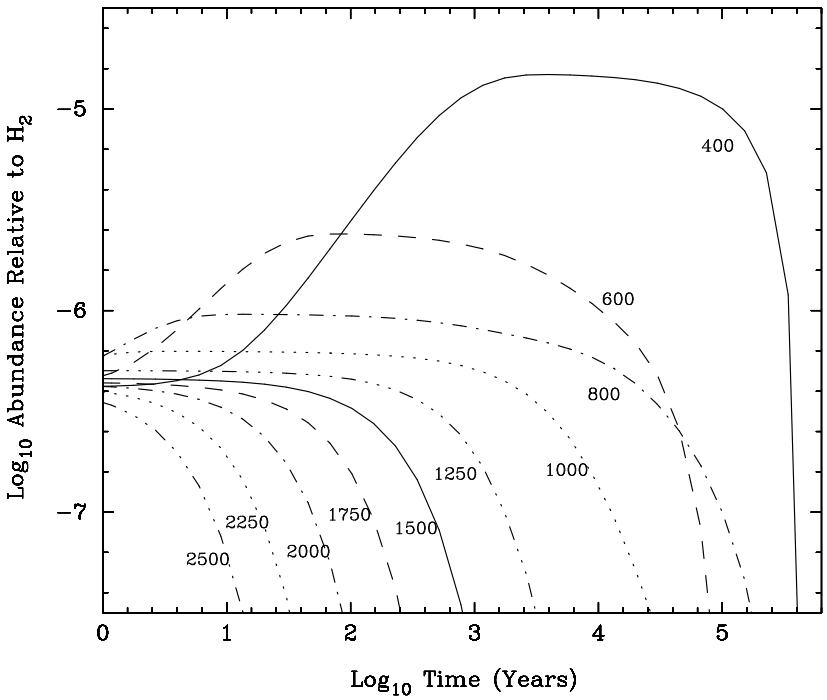

Fig. 5.— Abundance of O_2 as a function of time and gas temperature. The times listed on the abscissa are times after $\sim 10^5$ years of evolution with $T_{gas} = 30$ K (see Section 4.1).

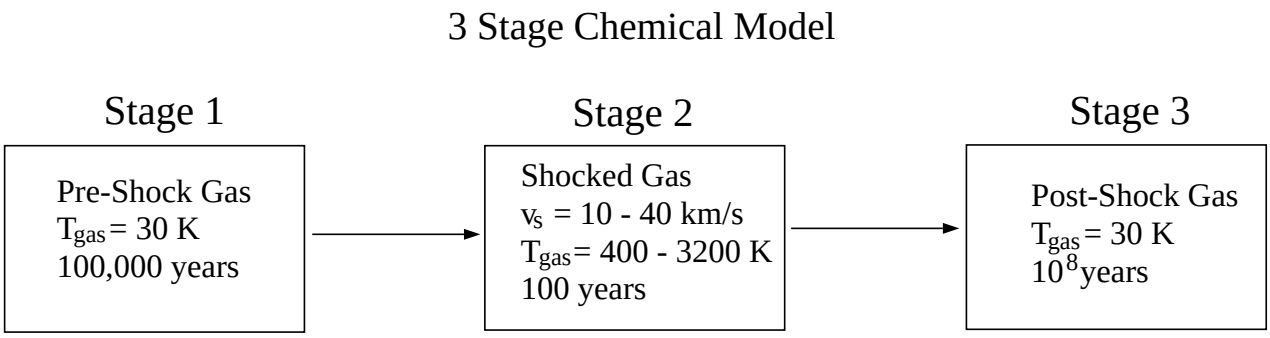

Fig. 6.— Schematic demonstrating the physical evolution of the three-stage chemical model of pre-shock, shocked, and post-shock gas. In all stages the density, visual extinction, and UV field enhancement are kept constant at $n_{H_2} = 10^5$ cm^{-3}, $A_V = 10$ mag, $G_o = 1$.

subjected to non-dissociative shocks as one with several potentially episodic evolutionary stages. The first stage of evolution is simply quiescent chemical and physical evolution. The gas starts its chemical evolution at low density with mostly atomic constituents and proceeds towards higher density with an increasing molecular composition. At some time the cloud undergoes a period of star formation and the protostars alter the local environment through radiation, winds, and outflows. The second stage of evolution occurs when a parcel of molecular gas is processed by a shock. After the passage of a shock, the gas rapidly cools, and the pre-shock time-dependent chemistry begins to be re-established. Thus the post-shock chemistry represents the third evolutionary stage. For a given parcel of gas, these three stages can be repeated, provided that star formation is still active in nearby regions (c.f. Charnley et al. 1988a,b).

To account for this picture, we have constructed a three-stage chemical model, shown schematically in Figure 6. In Stage (1) we use a pseudo-time dependent calculation of the chemical evolution in which the gas is initially atomic and the physical conditions for quiescent gas are those described earlier. This evolution continues with constant physical properties until $t = 10^5$ years when the gas undergoes a 20 km s^{-1} non-dissociative shock, which heats the gas and raises the gas temperature. At the completion of Stage (1), Stage (2) is started by re-initializing the chemical evolution and raising the gas temperature to the maximum value expected for a 20 km s^{-1} shock ($T_{gas} \approx 1000$ K; see Figure 1). In this fashion, the chemical abundances after 10^5 years of quiescent evolution are the initial conditions for the second stage. Based on the discussion in the previous section, we allow the evolution to continue at high temperature for 100 years. After 100 years, Stage (3) is begun and the chemistry is re-initiated with the abundances of 100 years of evolution at elevated temperatures providing the initial abundances. For the third stage we use the original gas temperature ($T_{gas} = 30$ K) and allow the chemistry to re-equilibrate. Through each of these stages, pre-shock (Stage 1), shock (Stage 2), and post-shock (Stage 3), only the temperature is altered in step-wise fashion, the other

physical properties (n_{H_2}, G_o, A_V) remain constant. The step-wise time evolution of temperature is a simple approximation of the shock temperature profile shown in Figure 2. As a check on these results we have also run a more complex multi-stage model using this temperature profile and we find that the results which we present in the following paragraphs are unaltered.

4.3.1. Pure Gas-Phase Chemistry

We first examine the three-stage chemical model using only the gas-phase chemical network. Figure 7 presents the results from a three-stage chemical model of a 20 km s^{-1} shock impacting on quiescent gas. In this figure the top panel presents the pre-shock chemical evolution (Stage 1), the middle panel the evolution in shocked gas (Stage 2), and the bottom panel the chemistry of the post-shock gas layer (Stage 3). *Note that the temporal range is different for each panel.*

Examining Figure 7 we observe that the chemical abundances in Stage (1) are quite similar to that observed in Figure 3; carbon is slowly processed into CO and the abundances H_2O and O_2 steadily increase. In Stage (2) the temperature is raised, and the H_2O abundance quickly rises to incorporate all of the oxygen that is not locked into CO. The formation of H_2O from O is preceded by formation of OH, which accounts for the sharp rise and decline in the hydroxyl abundance. However, even at 1000 K, the abundances of O_2 and CO are unchanged. In the post-shock evolution (Stage 3), the abundances of most species do not change for $\sim 10^4$ years. During this time there is a noticeable increase in the abundance of atomic oxygen, suggesting that even for times $< 10^5$ years there is some destruction of H_2O. But, for these early times, the abundance of atomic oxygen is more than an order of magnitude below that of H_2O. After $\sim 4 \times 10^5$ years of low-temperature evolution the chemistry dramatically changes as the abundance of water rapidly drops and the "normal" chemistry, with CO, O, and O_2 as the dominant oxygen reservoirs, is re-asserted. At this time the abundance of CO also exhibits a small drop followed by an immediate increase, which is due to CO reacting with OH (producing CO_2). This reaction has been measured at low temperatures in the laboratory (Frost, Sharkey, & Smith 1991).

In Figure 7 the quiescent stage is allowed to evolve for 10^5 years, if this stage is allowed to evolve for 10^6 years, or even 10^7 years, the abundances of a few selected species in the subsequent stages would be altered. Examining the full quiescent evolution shown in Figure 3, if the first stage evolves beyond 10^5 years, the abundance of atomic carbon is lowered, while molecular oxygen will be more abundant. If the shock is not strong enough to destroy O_2, the larger O_2 abundance would trap oxygen in molecular form and produce a lower H_2O abundance in the shock and post-shock stages.

For $n_{H_2} = 10^5$ cm^{-3}, the timescale for the re-assertion of low-temperature chemistry, τ_{ra}, is $\sim 4 - 7 \times 10^5$ years. In Figure 8 we examine the dependence of τ_{ra} on density for three-stage models run with $n_{H_2} = 10^4, 10^5, 10^6, 10^7$ cm^{-3}. In this figure we present only the water abundance in the post-shock stage. Even though chemical interactions occur with greater frequency at higher density, the chemical relaxation timescale does not depend on the density. This is a result of cosmic-ray driven chemistry. The principle mechanism for re-distribution of water back to other oxygen-bearing species is through the following two reactions:

$$H_2O + H_3^+ \rightarrow H_3O^+ + H_2. \qquad \text{(R5)}$$

$$H_2O + HCO^+ \rightarrow H_3O^+ + CO. \qquad \text{(R6)}$$

The first channel is important at early times, but the second channel dominates at late times. Because of the large abundance of water, the abundances of HCO^+ and H_3^+ decrease in the shock

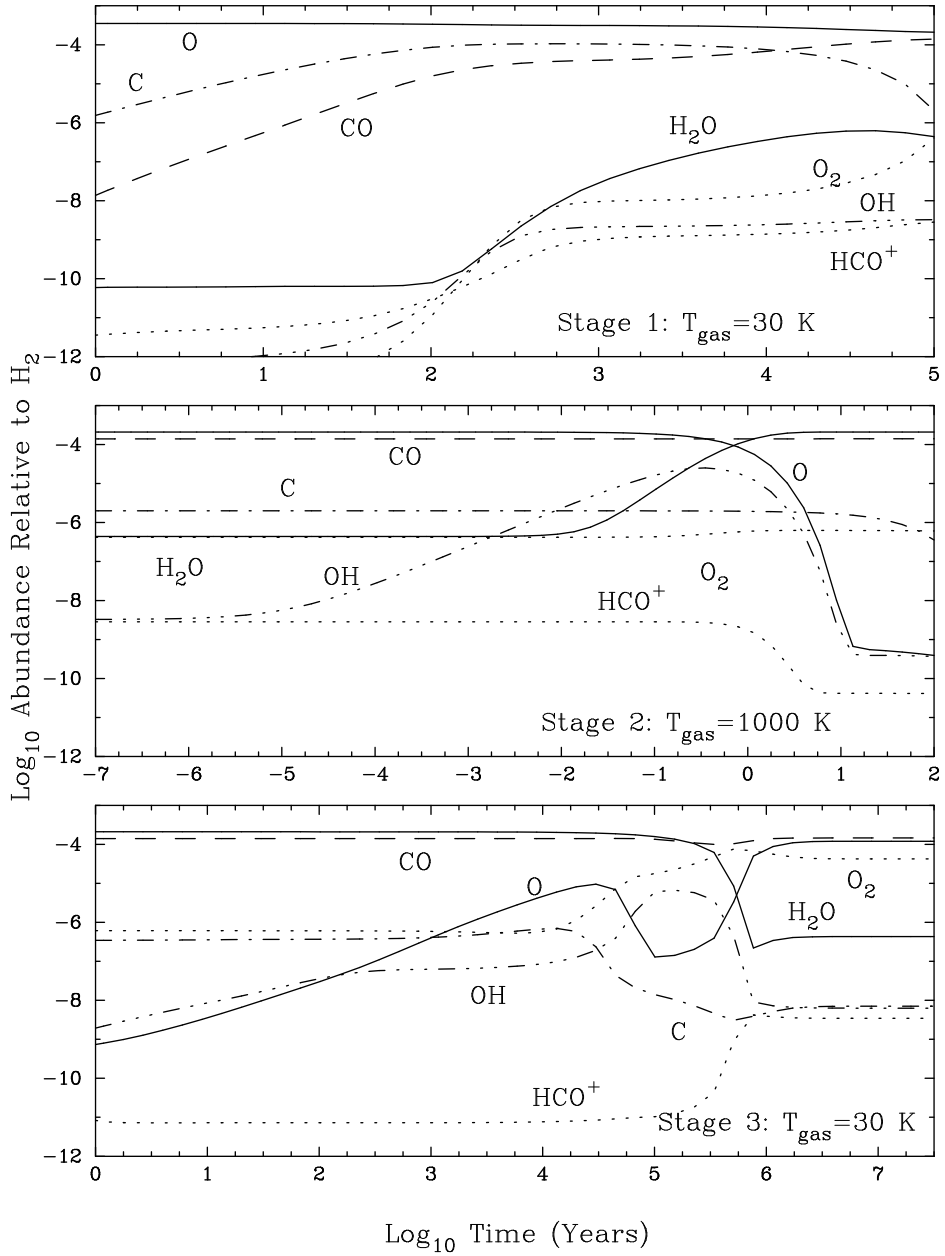

Fig. 7.— Evolution of chemical abundances relative to H_2 in the pure gas phase three-stage model as a function of time for simple carbon- and oxygen-bearing molecules (C, CO, O, OH, O_2, H_2O, HCO^+). Stage 1 (top panel) represents the pre-shock stage with $T_{gas} = 30$ K, Stage 2 (middle panel) is the shock stage with a higher gas temperature ($T_{gas} = 1000$ K), and Stage 3 (bottom panel) the post-shock stage with $T_{gas} = 30$ K. Note that the time axis for each panel covers a different range and shows the full evolution of chemical abundances from one stage to the next.

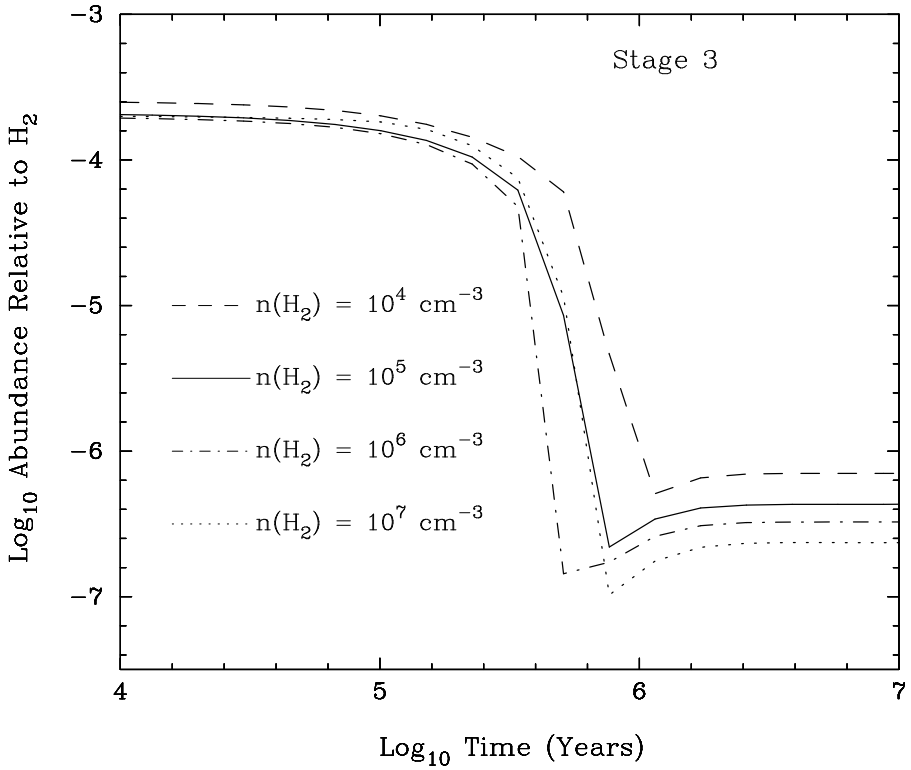

Fig. 8.— Evolution of H_2O abundance relative to H_2 in Stage 3 shown for $n_{H_2} = 10^4$, 10^5, 10^6, and 10^7 cm^{-3}.

phase. This effect on HCO^+ is shown in Figure 7. However, in the third stage at $t > 10^5$ years, the abundance of HCO^+ and H_3^+ begin to increase and water begins to be efficiently destroyed through the above reactions. Subsequently, the destruction of HCO^+ and H_3^+ decreases and the process begins to feed itself and the water abundance rapidly drops.

The lack of a dependence of τ_{ra} on density is also an important clue because, while the fractional abundance of H_3^+ depends on the density, the space density of H_3^+ ($x(H_3^+)n_{H_2}$) is constant with density (Lepp, Dalgarno, & Sternberg 1987). Because τ_{ra} is tied to the abundance of H_3^+, it will depend on the cosmic-ray ionization rate. In these calculations we have used an ionization rate of $\zeta_{H_2} = 10^{17}$ s^{-1}; for an ionization rate a factor of 5 higher, the timescale decreases approximately by a factor of 5.

4.3.2. Gas-Phase Chemistry Including Gas-Grain Interactions

Figure 9 presents the three-stage model run for $n_{H_2} = 10^5$ cm^{-3}, including grain surface molecular depletion and desorption. For these models we have set the dust temperature equal to the gas temperature $T_{dust} = T_{gas} = 30$ K. When the gas temperature is raised in Stage 2, the dust temperature is kept constant (c.f. Draine, Roberge, & Dalgarno 1983). The dominant desorption mechanism in this model is thermal evaporation from 30 K dust grains. The desorption rate is $k(H_2O)_{evap} = 7.2 \times 10^{-15}$ s^{-1} (see Bergin, Langer, & Goldsmith 1995). In this model we allow for the depletion of molecular species onto grain surfaces and account for some desorption, but we do not allow species to react on the grain surfaces. For water-ice this assumption is not unreasonable because H_2O is a stable endpoint in models of surface chemistry (c.f. Tielens and Hagen 1982) and the majority of gas phase H_2O depletion will occur in the post-shock layer when the water abundance has been raised by the shock. In addition, icy grain mantles may be removed inside shocks (through sputtering) such that all of the oxygen will eventually exist in the gas phase in the form of water. Thus, water created by the high–temperature shock will deplete back onto the mantle directly from the gas phase and will not be formed through grain surface reactions. For the three-stage model we do not

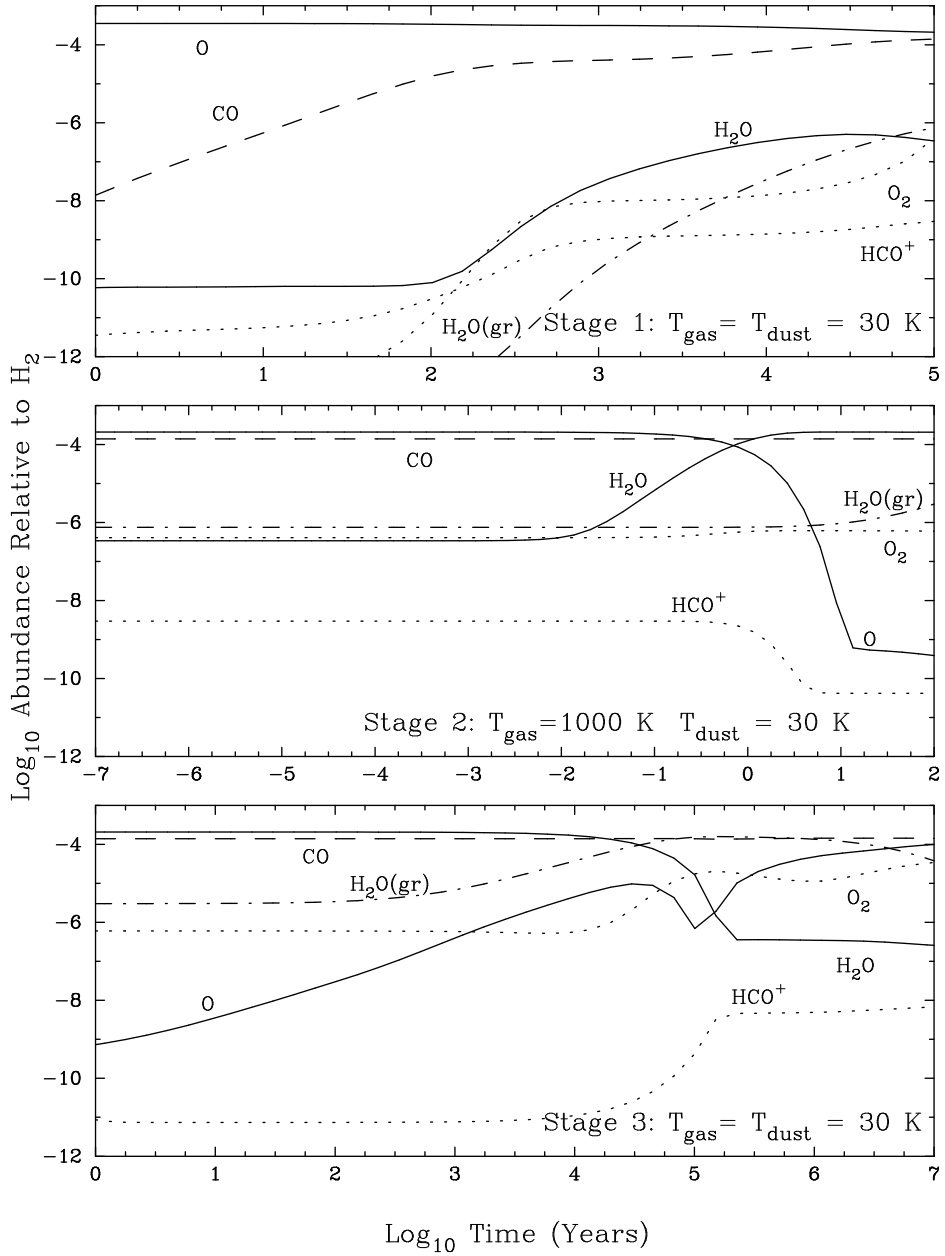

Fig. 9.— Evolution of chemical abundances in the gas-grain three-stage model as a function of time for simple carbon- and oxygen-bearing molecules (C, CO, O, O_2, H_2O, HCO^+). All abundances are relative to H_2. This model includes molecular depletion and desorption from grain surfaces and the abundance of H_2O on the grain surface (H_2O(gr)) is presented. Stage 1 (top panel) represents the pre-shock stage with $T_{gas} = 30$ K, Stage 2 (middle panel) is the shock stage with a higher gas temperature ($T_{gas} = 1000$ K), and Stage 3 (bottom panel) the post-shock stage with $T_{gas} = 30$ K. Note that the time axis for each panel covers a different range and shows the full evolution of chemical abundances from one stage to the next.

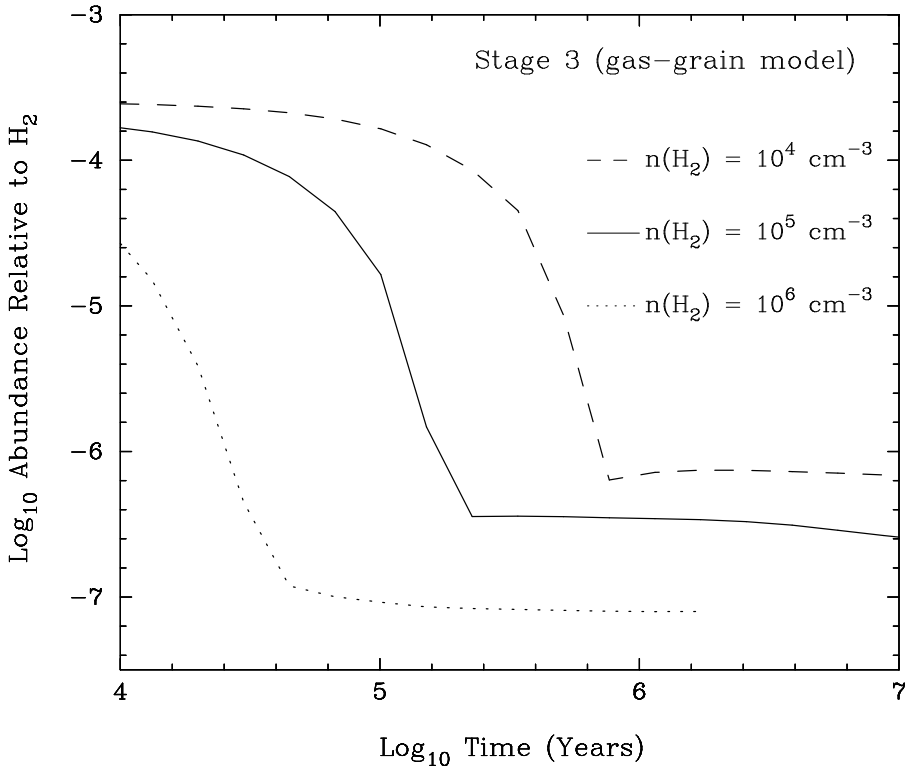

Fig. 10.— Evolution of H_2O abundance in Stage 3 from the gas-grain model shown for $n_{H_2} = 10^4$, 10^5, and 10^6 cm^{-3}. Abundances are relative to H_2.

account for any sputtering of the mantle inside the shock, but we will account for sputtering in the more general model presented later.

The quiescent evolution shown in the top panel of Figure 9 is not appreciably different from that seen in the pure gas-phase case. However, there is slow but steady accretion of water from the gas phase, such that by $t = 10^5$ years water is more abundant on the grain surface than in the gas phase. In contrast, due to lower grain surface binding energies, and therefore enhanced evaporation rates, both O_2 and CO remain in the gas phase. In Stage 2 the evolution between gas-phase and gas-grain models is almost identical; all of the oxygen not in CO, or on grains, is processed into H_2O. In Stage 3 we see the largest differences. Here the abundance of gas-phase water exhibits a sharp decline at $t \sim 10^5$ years, which is less than τ_{ra} inferred from pure gas-phase chemistry. The decrease in gas-phase water abundance is the result of depletion onto grains, which has a timescale of $\sim 10^5$ years for this density. As a result, the abundance of water on grains at these times becomes quite large $\sim 10^{-4}$. At later times ($t > 10^6$ years), the abundance of H_2O on the grain surface decreases as the water molecules in the grain mantles begin to escape via thermal evaporation. Because CO and O_2 do not deplete, the oxygen chemistry is maintained in the gas phase and the overall gas-phase water abundance is only a factor of 2 or 3 below that of the pure gas-phase case. We note that similar chemical evolution will be observed for lower dust temperatures because both CO and O_2 will not deplete from the gas phase (due to cosmic-ray-induced heating), while the more tightly bound H_2O molecules will deplete from the gas phase (see Bergin & Langer 1997).

To examine the dependence of post-shock gas-grain chemistry on density, in Figure 10 we present Stage 3 for models run at three different densities, $n_{H_2} = 10^4, 10^5, 10^6$ cm^{-3}. This figure demonstrates that the inclusion of grains places a density dependence on τ_{ra}, which is a reflection of the depletion timescale for water. For $n_{H_2} = 10^4$ cm^{-3}, the depletion timescale is equal to τ_{ra} while for higher densities the depletion timescale is less than the gas-phase relaxation timescale. Lastly, due to the large abundance of water trapped on grains, the equilibrium chemistry for gas-grain models is never truly reasserted since the chemistry does not reach equi-

librium.

4.4. Monte-Carlo Model of Molecular Cloud Evolution

The results presented in Section 4.3 suggest that if the frequency of shock passages is similar to τ_{ra}, then the water abundance should be quite large ($\sim 10^{-4}$). In contrast, if the shock timescale is $\gg \tau_{ra}$, then the water abundance should be close to the lower values expected in quiescent gas ($\sim 10^{-7}$). In this sense, the abundance of H_2O is a measure of the physical shock history within a cloud – more so than the dynamical information contained in line profiles, which can be short-lived compared to the lifetime of the chemical legacy. Likewise, because O_2 is destroyed in very strong shocks, the abundance of O_2 may also chart the history of such shocks.

To examine the utility of using the abundance of H_2O and O_2 to trace the shock history of molecular gas we have created a more general model of shocks in clouds using a Monte-Carlo simulation. To construct the Monte-Carlo cloud model we use the 10 km s^{-1} shock timescales determined in Section 3 for massive star-forming clouds and the chemical-dynamical model discussed in Section 2. In this model we allow the chemistry to evolve in steps of 10^4 years. If the shock timescale is $< \tau_s >= 10^6$ years, then during each time interval there is a 1 percent chance that the gas will experience a shock. This model is similar to the three-stage model, except that the time evolution of each stage is 10^4 years. As before, when a shock passes (determined by the generated random number), it is assumed that in all cases the period of elevated temperatures is 100 years; for all other times it is assumed that $T_{gas} = 30$ K. As a consequence of the momentum driven winds discussed in Section 3, we assume that the frequency of shocks faster than a given velocity is inversely proportional to that velocity. Thus 20 km s^{-1} shocks occur with a frequency that is a factor of two below that for shocks faster than 10 km s^{-1} shocks. The correspondence between the shock strength (velocity) and post-shock temperature is presented in Figure 1. If $v_s > 45$ km s^{-1} we account for the possibility of *dissociative* shocks and destroy all molecular abundances. The next cycle is then begun with the atomic initial abundances. The entire model is continued for a total of $\sim 10^8$ years or $\sim 10,000$ cycles.

The computations required to run thousands of cycles is too time consuming to use the full UMIST database. We therefore constructed a smaller network of 26 species and 145 reactions. This small network contained all of the important high- and low-temperature pathways to form carbon and oxygen species and was tested against a sample run that made use of the entire UMIST database, with no significant differences found.

Finally, models of shocked molecular gas have found that species can be desorbed from the grain mantle, or even the grain core, in shocks through sputtering or grain-grain collisions (c.f. Draine, Roberge, & Dalgarno 1983; Schilke et al. 1997; Caselli, Hartquist, & Havnes 1997). The amount of gas removed depends on the shock velocity and differs between various models. Based on the results of Caselli et al. (1997) we assume that shocks with $v_s \geq 15$ km s^{-1} will entirely remove the grain mantle. In these models we do not explicitly include a sputtering term, but rather simulate these effects by raising the dust temperature to 100 K. This will increase the rate of thermal evaporation and rapidly desorb mantle species.

4.4.1. Pure Gas-Phase Chemistry

In Figure 11 we show the number of shocks in 5 km s^{-1} bins that are generated by the Monte-Carlo cloud simulation with $< \tau_s >= 10^6$ years (shaded histogram) and 10^7 years (filled histogram). From the discussion of shock timescales in Section 3, $< \tau_s >= 10^6$ years is a value appropriate for regions of massive cluster formation (e.g., OMC-1), while $< \tau_s >= 10^7$ years is inferred for general GMC core material (e.g., Mon

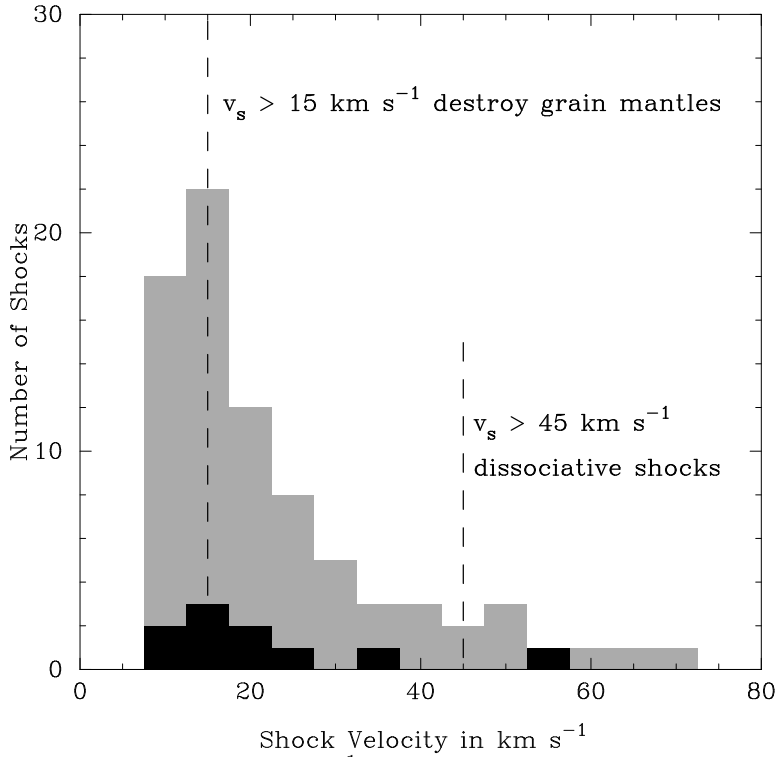

Fig. 11.— Number of shocks in 5 km s^{-1} bins from Monte-Carlo model run for $\sim 10,000$ cycles. Two models are shown, $\tau_s = 10^6$ (shaded histogram) and 10^7 years (filled histogram).

R2 or L1641). In both cases, the spectrum of shocks is heavily weighted towards lower velocities, but there are several fast dissociative shocks, even for $< \tau_s >= 10^7$ years. There are a few shocks with velocities higher than 80 km s^{-1}, but they are not included in this figure.

Figure 12 shows the full time dependence of the water abundance from the gas-phase Monte-Carlo model with $< \tau_s >= 10^6$ years (top panel) and 10^7 years (bottom panel) using the shock spectrums shown in the previous figure. For $< \tau_s >= 10^6$ years, the water abundance increases for the first 10^5 years and at $t \sim 10^6$ years sharply rises as the gas is shock-heated. The abundance decreases in the post-shock gas and goes through a series of successive shock heating and cooling events. The vertical lines that extend below $x(H_2O) = 10^{-12}$ are the result of dissociative shocks. Overall, the water abundance varies between $x(H_2O) \sim 10^{-6}$ and 10^{-4}, with an average abundance of $\sim 10^{-5}$. For a longer shock timescale (bottom panel), the water abundances show similar variations, but the effects are not as dramatic.

We have computed the time-averaged H_2O and O_2 abundances in the model presented in Figure 12 and these results are shown in Figure 13. To create this plot we compute a running average as a function of time, weighting the abundance by the length of time it remains at a given value. In this figure we also present the time-averages for another Monte-Carlo model run with $< \tau_s >= 5 \times 10^6$ years. For $< \tau_s >= 10^6$ years, the time-averaged water abundance converges to $\sim 10^{-5}$. For other, longer shock timescales, the water abundance takes longer to converge to a single value, but the overall amount of water is clearly dependent on the shock timescale. These effects can be quite large for $< \tau_s >$ greater than 10^7 years; the average water abundance will be at least a factor of five below the value for $< \tau_s >= 10^6$ years. It is also notable that even when the shock timescale is 10^7 years, the frequency of shocks is high enough that the time-averaged water abundance is greater than that expected for steady-state chemistry in quiescent gas (compare with Figure 1 where $x(H_2O) \sim 6 \times 10^{-7}$). In contrast, because the frequency of shocks with velocities high enough to destroy O_2 within the cooling time is low, the abundance of O_2 has a negligible dependence on the shock timescale.

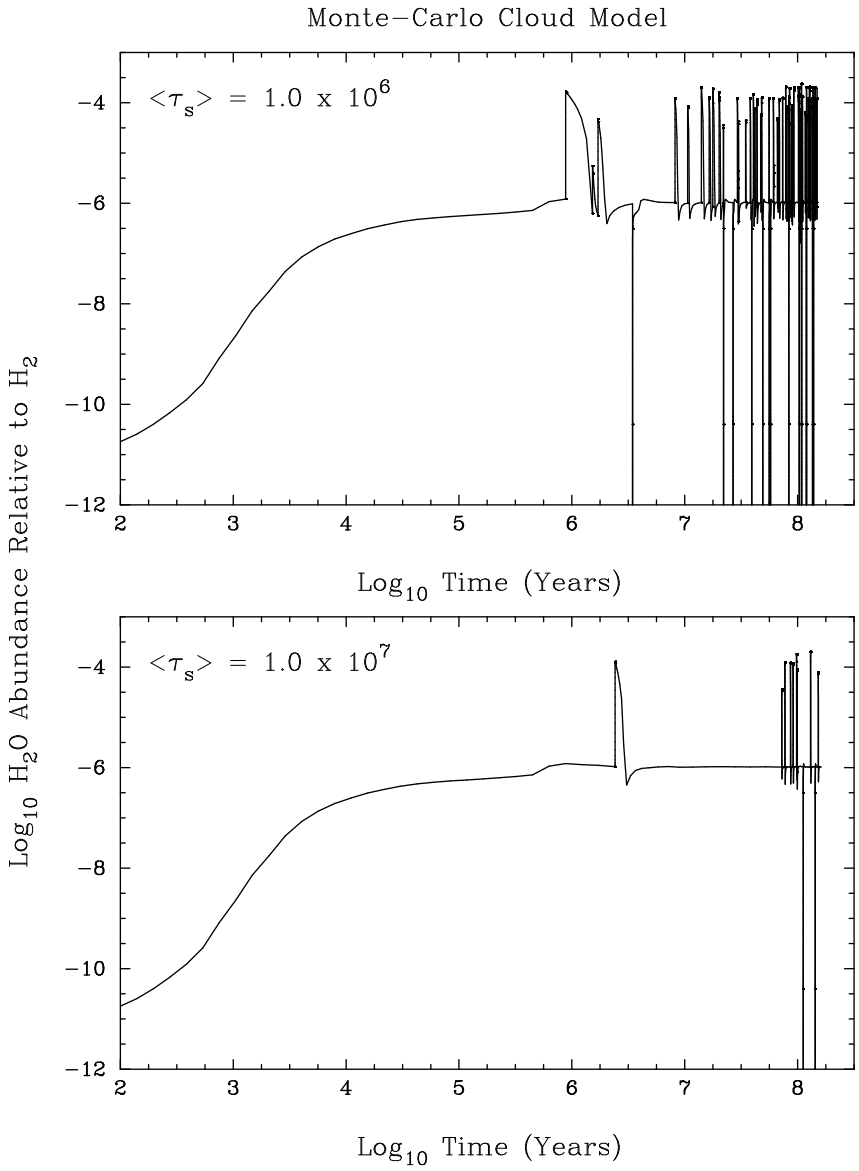

Fig. 12.— Abundance of H_2O relative to H_2 shown as a function of time for the Monte-Carlo cloud model. The top panel presents the chemical evolution for $\tau_s = 10^6$ years and the bottom panel for $\tau_s = 10^7$ years. The vertical lines extending to abundances below 10^{-12} are dissociative shocks.

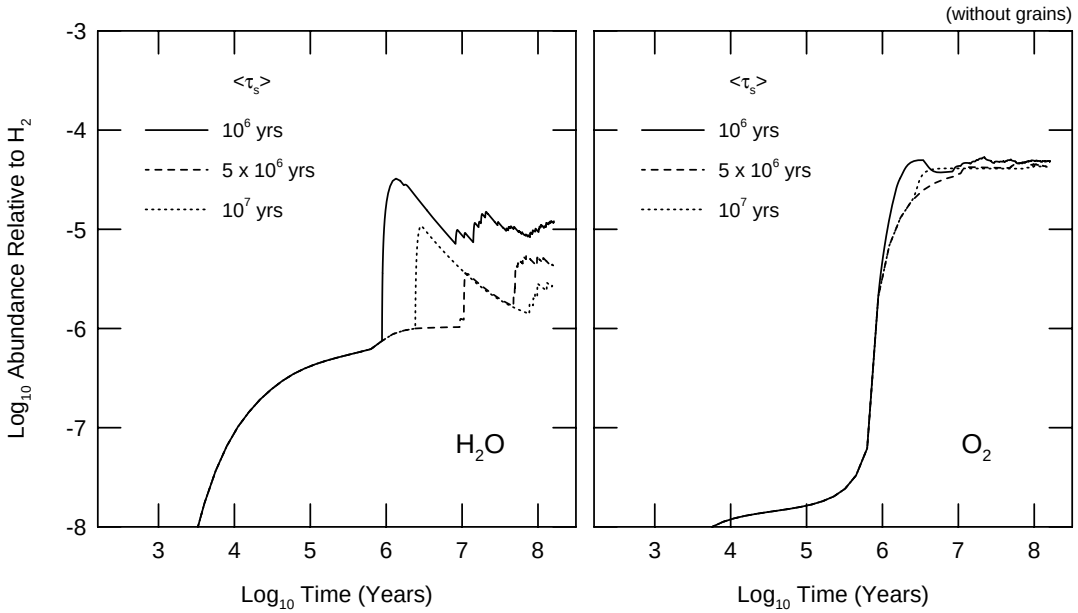

Fig. 13.— Time average abundances of H_2O and O_2 from Monte-Carlo cloud models run with variable shock timescales. This model is for pure gas-phase chemistry at $n_{H_2} = 10^5$ cm^{-3} and all abundances are calculated as relative to H_2. The time-averaged abundances are calculated as a running average, weighted by the amount of time the abundance remains at a given amount.

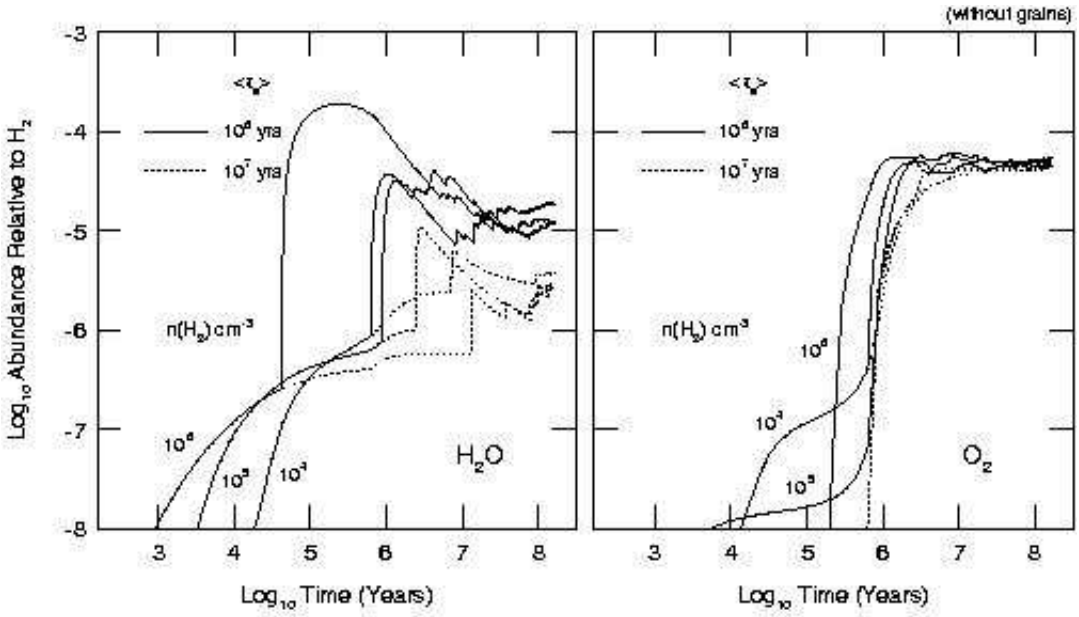

Fig. 14.— Time averaged H_2O and O_2 abundances (relative to H_2) from Monte-Carlo models run with two separate shock timescales and three different densities.

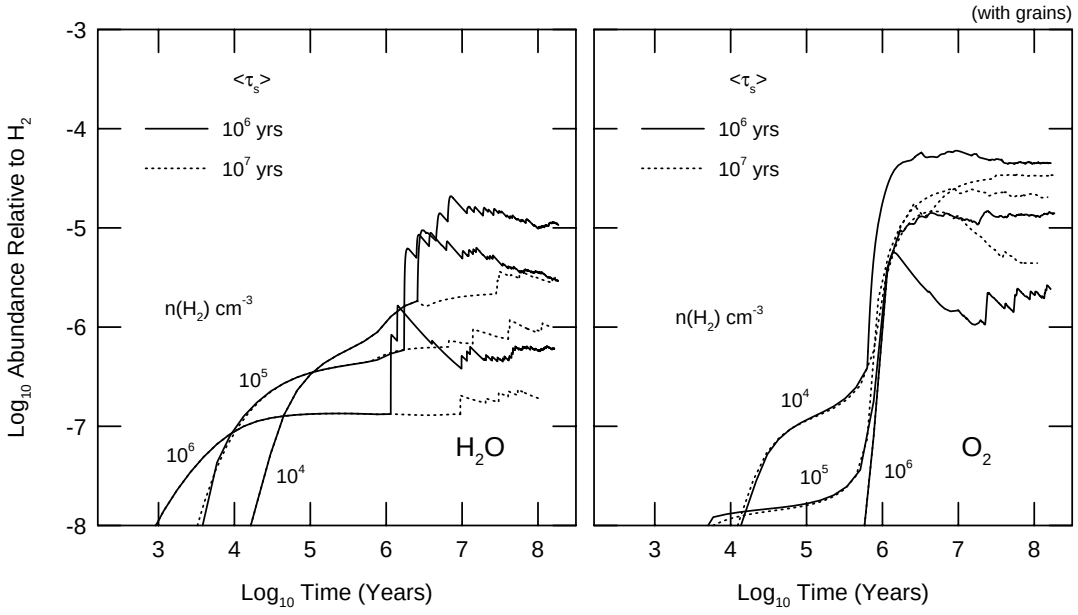

Fig. 15.— Same as in Figure 13, but for gas-grain Monte-Carlo model.

Figure 14 presents the time-averaged abundances for models run at $< \tau_s >= 10^6$ and 10^7 years for three different densities. The results shown in this figure confirm the earlier finding that for pure gas-phase chemistry and a constant cosmic-ray ionization rate, the chemical relaxation timescale has little dependence on the density. Similarly, the time-averaged H_2O abundance is not dependent on density. While the relaxation timescale does not depend on the density it does have a dependence on the cosmic-ray ionization rate (see discussion in Section 4.3.1). The relaxation timescale is inversely proportional to the ionization rate, such that a Monte Carlo model with a shock timescale τ_s and cosmic ray ionization rate of $\zeta_{H_2} = 10^{17}$ s^{-1} would roughly apply for a model with a shock timescale $< \tau_s >' = < \tau_s > /(\zeta'_{H_2}/10^{-17}s^{-1})$, where ζ'_{H_2} is a different cosmic ray ionization rate.

4.4.2. Gas-Phase Chemistry Including Gas-Grain Interactions

The time-averaged abundances calculated in the Monte-Carlo model, which include interactions between the gas phase with grain surfaces, are shown in Figure 15. These results are presented for three densities, $n_{H_2} = 10^4$, 10^5, 10^6 cm^{-3} and two shock timescales $< \tau_s >= 10^6$ and 10^7 years. As before, species are fully evaporated from the grain mantles if shock velocities exceed 15 km s^{-1}. The inclusion of depletion onto grains introduces a density dependence into the overall water abundance. Although the H_2O abundance does converge to a single time-averaged value, this value does have a dependence on the shock timescale. Therefore, to compare these results with observations, prior information about the density is required in order to differentiate between the various solutions. For molecular oxygen, the inclusion of gas-grain interactions introduces a dependence on the average abundance with density (because of the increasing depletion rate with increasing density). However, the time-averaged O_2 abundance is not as strongly dependent on the shock timescale.

5. Discussion

5.1. Comparison with Observations

Our results demonstrate that the *time-averaged* abundance of H_2O is a sensitive function of the rate at which molecular gas is subjected to shocks. In order to properly interpret these

results it is useful to consider how the time-averaged abundances relate to observations of water in a giant molecular cloud (GMC). The gas inside a star-forming cloud can roughly be divided into three categories: (1) quiescent material that has been relatively unaffected by current or previous epochs of star formation; (2) gas that is being physically and/or chemically affected by current star formation; and, (3) as suggested here, gas that has been affected by a previous generation of star formation and is in the process of chemically and dynamically evolving back to a quiescent state. Observations of H_2O toward molecular material associated with each of these categories should find abundances varying from as low as $x(H_2O) \sim 10^{-6}$ in (1), and ranging upwards to $\leq 10^{-4}$ in (2) and (3). *A single pointed detection of H_2O emission in a GMC can therefore be represented by a single stage of the three-stage or Monte-Carlo models (quiescent, shock, post-shock). Because star formation will be spread throughout a cloud or core, the time-averaged abundance therefore refers to water abundances averaged over an area that contains both quiescent material and any associated gas currently being affected by local star formation. Thus the average abundance over a cloud (cloud-average) is comparable to the time-averaged abundances in the Monte-Carlo cloud model.* This average abundance might not necessarily apply to an entire GMC complex (e.g. Orion, Gem OB1), which can extend for several square degrees on the sky, but may apply to several dense cores within a single cloud. Regions with high star-formation rates, such as OMC-1 which is associated with the Trapezium cluster (see Section 3), might be expected to have a higher probability for strong shocks, and therefore a high cloud-averaged water abundance. Cores with lower star-formation rates, such as L1641 also in Orion, would have low cloud-averaged water abundances.

To test our model's ability to constrain the history of molecular clouds it is important to obtain maps of the water emission over large spatial scales in GMC cores. Because of the strong absorption by atmospheric water vapor, observations of H_2O in the ISM are extremely difficult. As a result, the small number of detections of water in molecular clouds have typically been taken towards single lines of sight mostly containing luminous protostars. The very convincing detections of water by ISO provide the greatest evidence for high water abundances in hot gas, with $x(H_2O) \sim 1-6\times10^{-5}$ inferred towards hot stars (Helmich et al. 1996; van Dishoeck & Helmich 1996) and HH54 (Liseau et al. 1996). Towards Sgr B2 Zmuidzinas et al. (1994) observed $H_2^{18}O$ in absorption with the Kuiper Airbourne Observatory (KAO), while Neufeld et al. (1997) observed H_2O in emission using ISO. Combining these observations with previous ground based detections Neufeld et al. (1997) estimate an abundance of $x(H_2O) = 3.3\times10^{-7}$ for the cooler outer parts of Sgr B2 and $x(H_2O) \sim 5\times10^{-6}$ in the hot core. These observations are important not only because H_2O was detected in dense gas, but also because there appears to be a range of water abundances. However, it is difficult to discern whether the enhanced water abundances are the result of high-temperature chemistry that occurs behind shocks, high-temperature chemistry appropriate to gas near young stars (c.f. Doty & Neufeld 1997), or evaporation of grain mantle species (see discussion in Section 5.2) and there is little information on the spatial distribution of the water emission.

There have been a few attempts to map the extended emission of water. Gensheimer, Mauersberger, & Wilson (1996) mapped emission of the quasi-thermal $3_{13} \rightarrow 2_{20}$ transition of $H_2^{18}O$ in both the Orion Hot Core and Sgr B2, and found that the emission originated in a compact region ($< 10''$). Cernicharo et al. (1994) and Gonzalez-Alfonso et al. (1995) find evidence for widespread water emission in Orion and W49N using the $3_{13} \rightarrow 2_{20}$ masing transition of H_2O. In Orion they argue that the water abundance is

quite high, $x(H_2O) > 10^{-5}$, over an extended $50'' \times 50''$ region centered on BN-KL and the Orion Nebular Cluster. From these results, the cloud-averaged water abundance for the central regions of the Orion core near the Orion Nebular Cluster is $\gtrsim 10^{-5}$ which, using Figures 11 and 12 ($n_{H_2} = 10^6$ cm^{-3}; Bergin, Snell, & Goldsmith 1996), is consistent with $\tau_s \sim 10^6$ years, as suggested in Section 3. However, the determination of abundances from masing transitions is a difficult task and these results must be viewed as suggestive until they are confirmed by mapping data obtained in other H_2O lines.

For molecular oxygen, which also suffers from strong absorption due to atmospheric O_2, the situation is even more uncertain. There exists only one tentative detection of $^{16}O^{18}O$ towards L134N by Pagani, Langer, & Castets 1993, which implies $x(O_2) \sim 4 - 8 \times 10^{-5}$. However, a search for $^{16}O^{18}O$ emission in different positions in L134N and other galactic sources by Maréchal et al. 1997 did not confirm this detection and provides only upper limits of $O_2/CO < 0.1$, which, assuming $x(CO) = 2.7 \times 10^{-4}$ (Lacy et al 1994), gives $x(O_2) < 3 \times 10^{-5}$. Searches, with similar negative results, have also been performed for molecular oxygen in extra-galactic sources with favorable redshifts (Goldsmith & Young 1989; Combes et al. 1991; Liszt 1992) finding $x(O_2) < 10^{-6}$. A recent study by Combes, Wiklind, & Nakai (1997) towards a z = 0.685 object provides the lowest limit to date of $O_2/CO < 2 \times 10^{-3}$. For our most realistic case, the Monte Carlo gas-grain model, we find the time-averaged O_2 abundance is $\sim 2 \times 10^{-5}$. Thus, the combined effects of shocks and gas-grain chemistry could lower O_2 abundances below the observed limits in Galactic sources, but another explanation is required to account for extra-galactic observations. The low time-averaged O_2 abundance suggests that these results could have some bearing on the high abundances of neutral carbon relative to CO (C/CO $\sim$ 0.1) that are observed towards a variety of star forming regions (c.f. Plume 1995, Schilke et al 1996). However, because the number of dissociative shocks which destroy CO is not high enough, the time-averaged carbon abundance in the models is well below the observed value.

The best opportunity to test these results will be offered by two spaceborne observatories, *The Submillimeter Wave Astronomy Satellite (SWAS)* (Melnick et al. 1995) and *ODIN* (Hjalmarson 1995), both of which should launch within the next year. *SWAS* and *ODIN* are capable of observing and mapping the fundamental transition $1_{10} \rightarrow 1_{01}$ of H_2O at 557 GHz and the $3,3 \rightarrow 1,2$ transition of O_2 at 487 GHz. These transitions have low upper state energies ($\sim$ 26 K) and should be readily excited in hot gas near star-forming sites and, more importantly, in the colder more extended material such as the ridge of dense gas in Orion (c.f. Ungerechts et al. 1997).

Besides the computation of averaged abundances from mapping observations, combined observations of H_2O and O_2 should be a powerful tool in examining the shock history of gas. This is demonstrated in Figure 16 where the water abundance is plotted versus the molecular oxygen abundance for the Monte-Carlo model, including grain depletion and desorption (Section 4.4.2). In this plot, the majority of points trace an area of roughly constant water abundance of $x(H_2O) \sim 10^{-6}$, with the O_2 abundance ranging between $x(O_2) = 3 - 30 \times 10^{-6}$. This area has, by far, the largest number of points and defines the "main-sequence" of quiescent chemistry. From this main sequence a shock will trace a line extending almost horizontally to the right, with constant O_2 abundance. Very strong shocks continue at the end of the horizontal line and extend down almost vertically, lowering the O_2 abundance for constant H_2O abundance. This dependence of horizontal and vertical lines occurs because the H_2O is created more efficiently than O_2 destruction (see Figures 3 and 4). This plot is a different way of examining the mod-

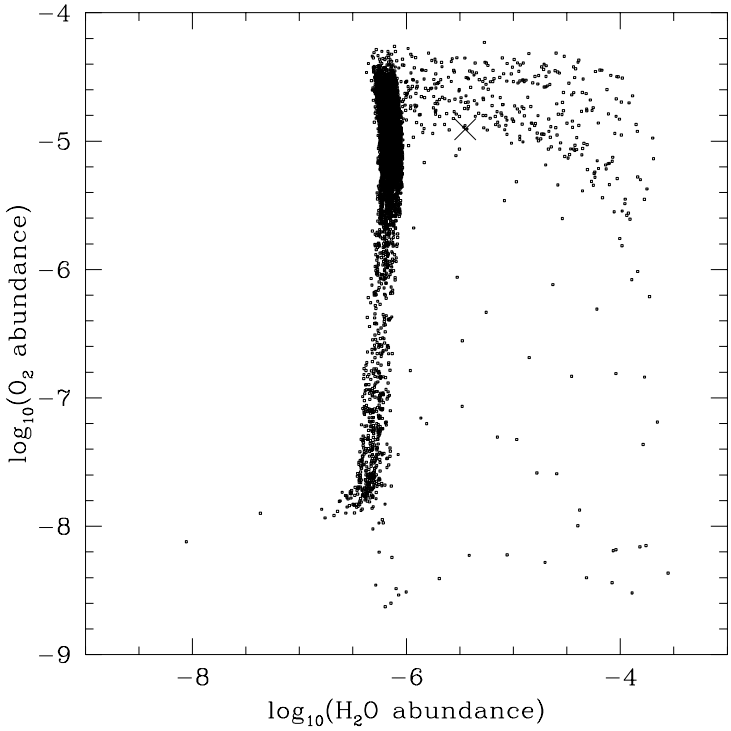

Fig. 16.— Points defining the plane of O_2 and H_2O abundances for the gas-grain Monte-Carlo model with $\tau_s = 10^6$ years and $n_{H_2} = 10^5$ cm^{-3}. The spread of plotted points has been artificially increased by smearing them by 0.2 dex so as to give a better sense of the density of points in different regions of the plot. The cross represents the mean (time-averaged) abundances.

els, as opposed to average abundances, because it presents the evolution in a continuous fashion; the various possible solutions define a plane that traces evolutionary tracks including quiescent chemistry through a broad range of shock strengths.

5.2. Post-Shock Chemistry and Water Ice Mantles

For comparison with previous modeling efforts, our three-stage model is similar to the episodic models presented in Charnley et al. (1988a,b). However, our model is simpler in that we do not model the formation process of a dense clump nor do we account for any mixing between shocked and non-shocked layers. Like their models, we find that the chemistry converges to well defined abundance values even when numerous cycles are repeated. Charnley et al. (1988a) also find that the water abundance varies greatly between shock and quiescent cycles, but they do not examine in detail the chemistry in the post-shock layer.

An interesting result in the gas-grain models is that the abundance of water on grain surfaces in post-shock gas is quite large $x(H_2O)_{gr} \sim 10^{-4}$. This abundance is quite close to that inferred for water ice along lines of sight towards background stars in Taurus, where $x(H_2O)_{gr} \sim 8 \times 10^{-5}$ (Whittet 1993). Thus, these results offer an alternative explanation for the large abundance of water in grain mantles – one that requires no grain surface chemistry! We stress that this mechanism may not be responsible for all H_2O observed on grains. Grain surface chemistry formation of H_2O must be considered – especially during cloud formation stages when the abundance of atomic hydrogen and oxygen is higher. There are also other potential desorption mechanisms that could be active and are not included in these models, such as grain mantle explosions induced by UV radiation (Schutte & Greenberg 1991) or water desorption via the infrared radiation field (Williams, Hartquist, & Whittet 1992). However, since most molecular clouds are very active star-forming sites, we suggest that caution must be applied when interpreting observa-

tions of ice mantles in molecular clouds as the sole result of grain surface chemistry. The interpretation of high gas-phase water abundances towards hot stars as the result of either high-temperature chemistry or grain mantle evaporation of H_2O is further obscured because water on grains may have been produced in an earlier shock episode. It is possible that the HDO/H_2O ratio could discriminate between water mantles created in shocks or in grain mantles and we are in the process of investigating this question (Bergin, Neufeld, & Melnick 1997).

The large abundance of water on grains, with CO remaining in the gas phase, will also alter the ratio of total carbon-to-oxygen (C/O) in the gas phase. Comparison of chemical theory with observations of molecular abundances in GMC cores associated with massive star formation has found that the chemical abundances of many species are best reproduced with C/O ratios greater than the solar value (> 0.4; Blake et al. 1987; Bergin et al. 1997). For chemical modeling this is the result of depletion of the initial abundance of oxygen relative to carbon, which reduces the abundances of small oxygen-bearing species that are major carbon destroyers in the gas phase. In the three-stage gas-grain model shown in Figure 7, the C/O ratio in the post-shock gas at $t \sim 10^5$ years is C/O ~ 0.7. It is difficult to gauge the effect of this on other species, because of the lack of certainty with regard to high-temperature reactions. It is therefore possible that the C/O ratios inferred in Blake et al. (1987) and Bergin et al. (1997) are indicative of the core formation process, which could involve gas temperatures rising high enough to convert atomic oxygen to water. In this case, these results suggest a simple mechanism to place large amounts of oxygen on grain surfaces while still keeping most of the carbon in the gas-phase.

Other molecular species, such as SO, SiO (Martín-Pintado, Bachiller, & Fuente 1992), and CH_3OH (Bachiller et al. 1995) have been observed with enhanced abundances in energetic outflows (see also Bachiller 1996; Bachiller & Pérez Gutiérrez 1997). These species are included in the three-stage chemical model presented in Section 4.3, but we do not present the results in detail here because of uncertainties in the high-temperature reaction rates. However, these results do have some bearing on the chemistry of these species in the post-shock layer. The formation pathway of CH_3OH in the gas phase is linked to a reaction of CH_3^+ with H_2O (Millar, Herbst, & Charnley 1991). Thus, it is possible that the enhanced abundance of water through high-temperature reactions could lead to larger CH_3OH abundances through this reaction. In the three-stage model, the CH_3OH abundance in the post-shock layer is $x(CH_3OH) = 1 - 5 \times 10^{-8}$ when the shock temperature ranges from 1000 to 2000 K. These abundances are at least an order of magnitude below values inferred in molecular outflows, which can be as high as $x(CH_3OH) \sim 10^{-6}$ (Bachiller et al. 1995). The mechanism of methanol enhancements may therefore be the result of grain mantle evaporation or an unidentified high- or low-temperature pathway. The abundance of CH_3OH accreted onto grain surfaces provides another constraint. In our model the abundance of CH_3OH ice in the grain mantle is only 0.1 percent of the water-ice abundance. This ratio is below that observed towards NGC 7538 or W33A where $x(CH_3OH)/x(H_2O) \sim 10-40$ percent (Allamandola et al. 1992). Our models do not set constraints on the chemistry of SO and SiO because the large abundances of these species in outflows may be the result of sputtering of grain refractory and/or mantle material (c.f. Schilke et al. 1997; Caselli et al. 1997).

When the abundances of these species are enhanced, through any mechanism, the high abundances will persist until the timescale for the individual molecule to deplete onto grain surfaces. If the dust temperature is high enough to keep a given species in the gas-phase, or for pure gas-phase chemistry, the lifetime will be $\tau_{ra} = 4 - 7 \times 10^5$ years. In these models all

SiO depletes onto grain surfaces at $\tau_{dep} \sim 10^4$ years (for $n_{H_2} = 10^5$ cm^{-3} and assuming a sticking coefficient of unity). For CH_3OH abundance enhancements we find that the depletion timescale for gas-grain chemistry is equal to that of H_2O ($\tau_{dep}(H_2O) \sim 10^5$ years). The disparity in post-shock lifetimes between CH_3OH, H_2O, and SiO suggests that differences might exist between younger outflows, perhaps those associated with so-called Class 0 sources, and the more evolved sources (e.g. Class I). A survey of such sources in these tracers might prove to be useful in probing the links between evolutionary effects observed in outflows and the relationship to the driving source. Another possibility is that differences could also be found within different components inside a single outflow (see Bachiller & Pérez Gutiérrez 1997).

The abundance of some molecular species, notably HCO^+ and N_2H^+, are adversely affected by the high water abundance. In Figure 7, for the three-stage model, the abundance of HCO^+ is decreased through reaction R6 when the water abundance is raised. Thus, the abundances of these two important molecular species should be anticorrelated. Because N_2H^+ also reacts with H_2O, a similar anticorrelated behavior would be found between the abundances of N_2H^+ and H_2O and may account for the low HCO^+ and N_2H^+ abundances in hot regions such as the Orion Hot Core (c.f. Blake et al. 1987) and in the L1157 outflow (Bachiller & Pérez Gutiérrez 1997).

6. Summary

We have investigated the use of simple oxygen-bearing molecules, H_2O and O_2, as tracers of the shock history of molecular gas. To this end, we have constructed a coupled chemical and dynamical model of dense molecular gas that is subject to heating by non-dissociative C-type shocks, and subsequently cools. To constrain the effects of MHD shocks on molecular gas we use the shock models of Kaufman & Neufeld (1996a,b). We have constructed two models and concentrate, in particular, on the chemistry in a layer of post-shock cooled gas. In the first model we examine the chemical evolution in three-stages: (1) as molecules form and increase in abundance within quiescent, pre-shock gas; (2) the rapid chemical changes precipitated by the passage of a C-shock; and, (3) the post-shock chemical evolution that occurs as the gas cools. The results of the three-stage model are combined with observational estimates of shock rates within molecular gas in regions of molecular outflows. A second, more general, model uses a Monte-Carlo method to examine the chemistry in a parcel of gas that is subject to random shock heating over a cloud lifetime. Because water is also an abundant molecule on the surfaces of interstellar grains, we have separately examined the pure gas-phase chemistry and the gas-phase chemistry including grain surface molecular depletion and desorption.

The principal results from this study are:

1) For $v_s > 10$ km s^{-1}, high temperature neutral-neutral chemical reactions are efficient at converting all of the available oxygen into H_2O within the post-shock region before the gas has an opportunity to cool. For lower shock velocities, the water abundance will not change significantly from its quiescent values due to the rapid post-shock cooling to temperatures less than those required to initiate these neutral-neutral reactions. This result is in agreement with previous investigations. Similarly, for $v_s >$ 26 km s^{-1}, all O_2 will be destroyed inside the shock within the cooling time.

2) For pure gas-phase models, the enhanced H_2O abundance behind a shock will decrease and the low-temperature chemistry will be reasserted at $\tau_{ra} \sim 4 - 7 \times 10^5$ years. As a result of cosmic-ray driven chemistry, τ_{ra} is nearly independent of the gas density. For models which include gas-grain interactions, a density dependence is found as the large abundance of water in the gas-phase will decrease though accretion onto grain surfaces at the depletion timescale. The depletion timescale has an inverse depen-

dence on the density and is less than τ_{ra} for $n_{H_2} > 10^5$ cm^{-3}.

3) We find that the time-averaged abundance of H_2O is a sensitive function of the shock frequency. This abundance is approximately the weighted average of the amount of time gas spends in the pre-shock, shocked, and post-shock stages respectively, and determines the average abundance of water mapped over a large region. Thus these models predict that the abundance of H_2O, and to a lesser extent O_2, can be used to constrain the physical history of molecular gas. The observations required to test these predictions can be performed from *The Submillimeter Wave Astronomy Satellite* and *ODIN*.

4) The abundance of water-ice on grain surfaces can be quite large in the post-shock gas layer. The abundance is often $x(H_2O)_{gr} > 10^{-4}$ and is comparable to that observed in molecular clouds. This offers an alternative method to create water-ice mantles without resorting to grain surface chemistry – passage of a C-type shock, followed by rapid hydrogenation of gas-phase oxygen, and subsequent depletion of water onto cold dust grains. Despite the large amount of water trapped on grains, the gas-phase chemistry is maintained because CO and O_2 do not deplete. This differential depletion of H_2O compared to CO and O_2 can also effectively raise the C/O ratio in the gas phase to values that are inferred from previous observational and theoretical comparisons of chemical abundances in GMC cores.

5) The abundance of a few molecular species are adversely affected by the high water abundances in shocked regions. In particular the abundances of N_2H^+ and HCO^+ are predicted to have abundances that are anticorrelated with changes in the water abundances.

We thank the referee R. Bachiller for a thorough review and some helpful comments. We also thank C. Lada and R. Snell for useful discussion on shock timescales in molecular clouds, and A. Dalgarno for discussions on chemical reactions. We are also indebted to M. Kaufman for kindly providing output from his shock models. E.A.B. and G.J.M. acknowledge the support of NASA grant NAGW-3147 from the Long-Term Space Astrophysics Research Program; and D.A.N. acknowledges the support of the Smithsonian subcontract SV-62005 from the SWAS program.

REFERENCES

Allamandola, L. J., Sandford, S. A., Tielens, A. G. G. M., & Herbst, T. M. 1992, ApJ, 399, 134

Bachiller, R. & Pérez Gutiérrez, M. 1997, ApJ, 487L, 93

Bachiller, R. 1996, Ann. Rev. Astron. Astrophys., 34, 111

Bachiller, R., Liechti, S., Walmsley, C. M., & Colomer, F. 1995, A&A, L51

Bachiller, R., Martín-Pintado, J., & Fuente, A. 1991, A&A, 243, L51

Bachiller, R., & Cernicharo, J. 1990, A&A, 239, 276

Bally, J., Devine, D., & Alten, V. 1996, ApJ, 473, 911

Bergin, E. A., Neufeld, D. A., & Melnick, G. J. 1997, in preparation

Bergin, E. A., & Langer, W. D. 1997, in press

Bergin, E. A., Goldsmith, P. F., Snell, R. L., & Langer, W. D. 1997, ApJ, in press

Bergin, E. A., Snell, R. L., & Goldsmith, P. F. 1996, ApJ, 460, 343

Bergin, E. A., Langer, W. D., & Goldsmith, P. F. 1995, ApJ, 441, 222

Blake, G. A., Sutton, E. C., Masson, C. R., & Phillips, T. G. 1987, ApJ, 315, 621

Carpenter, J. M., Snell, R. L., & Schloerb, F. P. 1995a, ApJ, 445, 246

Carpenter, J. M., Snell, R. L., & Schloerb, F. P. 1995b, ApJ, 450, 201

Caselli, P., Hartquist, T. W., & Havnes, O. 1997, A&A, in press

Cernicharo, J., González-Alfonso, Alcolea, J., Bachiller, R., & John, D. 1994, ApJ, 432, L59

Charnley, S. B., Dyson, J. E., Hartquist, T. W., & Williams, D. A. 1988a, MNRAS, 231, 269

Charnley, S. B., Dyson, J. E., Hartquist, T. W., & Williams, D. A. 1988b, MNRAS, 235, 1257

Combes, F., Wiklind, T., & Nakai, N. 1997, A&A, in press

Combes, F., Casoli, F., Encrenaz, P., Gerin, M., Laurent, C. 1991, A&A, 248, 607

Doty, S. D., & Neufeld, D. A. 1997, ApJ, in press

Draine, B. T. 1980, ApJ, 241, 1021

Draine, B. T., & McKee, C. F. 1993, Ann. Rev. Astron. Astrophys., 31, 373

Draine, B. T., & Roberge, W. G. 1982, ApJ, 259, 91L

Draine, B. T., Roberge, W. G., & Dalgarno, A. 1983, ApJ, 264, 485

Elitzur, M. & de Jong, T. 1973, A&A, 67, 323

Elitzur, M. & Watson, W. D. 1978, A&A, 70, 443

Elmegreen, B. G. 1992, in Star Formation in Stellar Systems, ed. G. Tenorio-Tagle, M. Prieto, & F. Sanchez (Cambridge: Cambridge University Press), 381

Flower, D. R., & Pineau des Forêts, G. 1995, MNRAS, 275, 1049

Frost, M. J., Sharkey, P., Smith, I. M. W. 1991, Faraday Discuss. Chem. Soc., 91, 305

Gensheimer, P. D., Mauersberger, R., & Wilson, T. L. 1996, A&A, 314, 281

Goldsmith, P. F. & Young, J. S. 1989, 341, 718

Goldsmith, P. F. 1987, in Interstellar Proceses, eds. D. J. Hollenbach & H. A. Thronson Jr. (Dordrecht: D. Reidel), 51

Goldsmith, P. F, Langer, W. D., & Wilson, R. W. 1986, ApJ, 303L, 11

González-Alfonso, E., Cernicharo, J., Bachiller, R., & Fuente, A. 1995, A&A, 293, L9

Graedel, T. E., Langer, W. D., & Frerking, M. A. 1982, ApJS, 48, 321

Guélin, M., Langer, W. D., & Wilson, R. W. 1982, A&A, 107, 107

Helmich, F. P., van Dishoeck, E. F., Black, J. H., de Graauw, Th., Beintema, D. A., Heras, A. M., Lahuis, F., Morris, P. W., & Valentijn, E. A. 1996, A&A, 315L, 173

Herbst, E., & Klemperer, W. 1973, ApJ, 185, 505

Hillenbrand, L. A. 1997, AJ, 113, 1733

Hjalmarson, Å 1995, in Physics and Chemistry of Interstellar Molecular Clouds, eds. G. F. Winnewisser and G. C. Pelz (Berlin: Springer-Verlag), 369

Jacq, T., Walmsley, C. M., Henkel, C., Baudry, A., Mauersberger, R., & Jewell, P. R. 1988, A&A, 228, 447

Kaufmann, M. J., & Neufeld, D. A. 1996, 456, 250

Kaufmann, M. J., & Neufeld, D. A. 1996, 456, 611

Knacke, R. F., & Larson, H. P. 1991, ApJ, 367, 162

Lacy, J. H., Knacke, R., Geballe, T. R., & Tokunaga, A. T. 1994, ApJ, 428L, 69

Lada, C. J. 1985, Ann. Rev. Astron. Astrophys., 23, 267

Lee, H.-H., Herbst, E., Pineau des Forêts, G., Roueff, E., & Le Bourlot, J. 1996, A&A, 311, 690

Lepp, S., Dalgarno, A., & Sternberg, A. 1987, ApJ, 321, 383

Liseau, R. et al. 1996, A&A, 315L, 181

Liseau, R., Sandell, G., & Knee, L.B.G. 1988, A&A, 192, 153

Liszt, H. S. 1992, ApJ, 386, 139

Marèchal, P., Pagani, L., Langer, W. D., & Castets, A. 1997, A&A, 318, 252

Margulis, M., & Lada, C. J. 1986, ApJ, 309, L87

Margulis, M., Lada, C. J., & Snell, R. L. 1988, ApJ, 333, 316

Martín-Pintado, J., Bachiller, R., & Fuente, A. 1992, A&A, 254, 315

Melnick, G. J., Dalgarno, A., Erickson, N. R., Fazio, G. G., Goldsmith, P. F., Harwit, M., Hollenbach, D. J., Koch, D. G., Neufeld, D. A., Schieder, R., Snell, R. L., Stauffer, J. R., Thaddeus, P., Tolls, V., & Winnewisser, G. F. 1995, in The Physics and Chemistry of Interstellar Molecular Clouds, eds. G. F. Winnewisser and G. C. Pelz (Berlin: Springer-Verlag), 352

Millar, T. J., Rawlings, J. M. C., Bennet, A., Brown, P. D., & Charnley, S. B. 1991, A&A Suppl. Ser.., 87, 585

Millar, T. J., Herbst, E., & Charnley, S. 1991, ApJ, 369, 147

Millar, T. J., Farquhar, P. R. A., & Willacy, K. 1997, A&AS, 121, 139

Morgan, J. A., Schloerb, F. P., Snell, R. L, & Bally, J. 1991, ApJ, 376, 618

Mullan, D. J. 1971, MNRAS, 153, 145

Neufeld, D. A., Zmuidzinas, J., Schilke, P., & Phillips, T. G. 1997, ApJ, 488, L141

Neufeld, D. A., & Melnick, G. J. 1987, ApJ, 322, 266

Pagani, L., Langer, W. D., & Castets, A. 1993, A&A, 274, L13

Plume, R. 1995, PhD Thesis, Univ. of Texas

Pineau des Forêts, G., Roueff, E., Schilke, P., & Flower, D. R. 1993, MNRAS, 262, 915

Prasad, S. S., & Huntress, W. T., Jr. 1980, ApJS, 34, 405

Prasad, S. S., Tarafdar, S. P., Villere, K. R., & Huntress, W. T., Jr. 1987, in Interstellar Processes, eds. D. J. Hollenbach and H. A. Thronson Jr. (Dordrecht: D. Reidel), 631

Rawlings, J. M. C., Hartquist, T. W., Menten, K. M., & Williams, D. A. 1992, MNRAS, 255, 471

Schilke, P., Walmsley, M., Pineau des Forêts, G., & Flower, D. R. 1997, A&A, 321, 293

Schilke, P., Keene, J., Le Bourlot, J, Pineau des Forêts, G., & Roueff, E. 1996, A&A, 294L, 17

Schutte, W. A., & Greenberg, J. M. 1991, 244, 190

Smith, D., & Spanel, P. 1993, J. Chem. Phys. Letts., 211, 454

Sundström et al. 1994, Science, 263, 785

Staude, H. J., & Elsässer H. 1993, A&A Rev, 5, 165

Sternberg, A. & Dalgarno, A. 1995, ApJS, 99, 565

Sundstrom, G. et al. 1994, Science, 263, 785

Tielens, A. G. G. M., & Hagen, W. 1982, A&A, 114, 245

Troland, T. H., & Heiles, C. 1986, ApJ, 301, 339

Ungerechts, H., Bergin, E. A., Goldsmith, P. F., Irvine, W. M, Schloerb, F. P., & Snell, R. L. 1997, ApJ, in press

van Dishoeck, E. F., & Helmich, F. P., A&A, 315L, 177

Vejby-Christensen, L., Andersen, L. H., Heber, O., Kella, D., Pedersen, H. B., Schmidt, H. T., & Zajfman, D. 1997, ApJ, in press

Warin, S., Castets, A., Langer, W. D., Wilson, R. W., & Pagani, L. 1996, A&A, 306, 935

Whittet, D. C. B. 1993, in Dust and Chemistry in Astronomy, eds. T. J. Millar & D. A. Williams (Bristol: Institute of Physics), 9

Willacy, K., Rawlings, J. M. C., & Williams, D. A. 1994, MNRAS, 269, 921

Williams, D. A., Hartquist, T. W., & Whittet, D. C. B. 1992, MNRAS, 258, 599

Williams, T. L., Adams, N. G., Babcock, L., Herd, C. R., & Geoghegan, M. 1996, MNRAS, 282, 413

Zmuidzinas, J., Blake, G. A., Carlstrom, J., Keene, J., Miller, D., Schilke, P., & Ugras, N. G. 1994, in *Proceedings of the Airborne Astronomy Symposium on the Galactic Ecosystem: From Gas to Stars to Dust*, ed. M. R. Haas, J. A. Davidson, & E. F. Erickson (San Francisco: ASP)

This 2-column preprint was prepared with the AAS LaTeX macros v4.0.